Missouri State University

BearWorks

MSU Graduate Theses

Summer 2019

Stream Channel Morphology and Riparian Forest Response to a 500-year Flood in the Missouri Ozarks

Joshua William Hess
Missouri State University, Joshua16@live.missouristate.edu

As with any intellectual project, the content and views expressed in this thesis may be considered objectionable by some readers. However, this student-scholar's work has been judged to have academic value by the student's thesis committee members trained in the discipline. The content and views expressed in this thesis are those of the student-scholar and are not endorsed by Missouri State University, its Graduate College, or its employees.

Follow this and additional works at: https://bearworks.missouristate.edu/theses

 Part of the Environmental Monitoring Commons, and the Geomorphology Commons

Recommended Citation

Hess, Joshua William, "Stream Channel Morphology and Riparian Forest Response to a 500-year Flood in the Missouri Ozarks" (2019). *MSU Graduate Theses*. 3435.
https://bearworks.missouristate.edu/theses/3435

This article or document was made available through BearWorks, the institutional repository of Missouri State University. The work contained in it may be protected by copyright and require permission of the copyright holder for reuse or redistribution.
For more information, please contact BearWorks@library.missouristate.edu.

STREAM CHANNEL MORPHOLOGY AND RIPARIAN FOREST RESPONSE TO A 500-YEAR FLOOD IN THE MISSOURI OZARKS

A Master's Thesis

Presented to

The Graduate College of

Missouri State University

In Partial Fulfillment

Of the Requirements for the Degree

Master of Science, Geospatial Sciences in Geography and Geology

By

Joshua William Hess

August 2019

Copyright 2019 by Joshua William Hess

STREAM CHANNEL MORPHOLOGY AND RIPARIAN FOREST RESPONSE TO A 500-YEAR FLOOD IN THE MISSOURI OZARKS

Geography, Geology, and Planning

Missouri State University, August 2019

Master of Science

Joshua William Hess

ABSTRACT

Climate change has increased the frequency of large floods in rivers draining the Ozark Highlands resulting in higher rates of channel sedimentation, bank erosion, and damage to infrastructure. This study assesses the effects of a large flood (>500-year RI) during April-May 2017 on riparian forests along six tributary streams in the North Fork of the White River watershed, Missouri. High-resolution (<8 cm) Unmanned Aerial Vehicle (UAV) imagery collected after the flood was used to identify riparian forest flood damage. Measurements of riparian forest flood damage calculated from the UAV imagery were verified through field surveys of damaged riparian trees. Geomorphic variables of valley confinement, sinuosity, substrate, and stream power were evaluated and used to explain the spatial distribution of riparian forest flood damage. In total over 1,000 damaged trees were identified at the sample reaches and canopy cover was reduced by up to 63%. Regression analysis showed positive relationships between riparian forest damage (total volume of damaged trees, volume of damaged trees per hectare, and canopy loss) with geomorphic variables such as confinement, sinuosity, substrate, and stream power. Mean ($R^2 = 0.67$) and cross-sectional ($R^2 = 0.90$) stream power accounted for the greatest percentage of variance in volume of riparian forest damage. Riparian forest damage peaked in the reaches with the largest drainage areas. UAVs have the potential to accurately assess riparian forest damage due to floods. However, more research on UAV measurement errors is needed to better evaluate UAV forest data. This information can be used to understand ecological disturbance by floods and inform land management practices in Mark Twain National Forest.

KEYWORDS: floods, riparian forests, Missouri Ozarks, fluvial geomorphology, UAV imagery

STREAM CHANNEL MORPHOLOGY AND RIPARIAN FOREST RESPONSE TO A 500-YEAR FLOOD IN THE MISSOURI OZARKS

By

Joshua William Hess

A Master's Thesis
Submitted to the Graduate College
Of Missouri State University
In Partial Fulfillment of the Requirements
For the Degree of Master of Science, Geospatial Sciences in Geography and Geology

August 2019

Approved:

Robert T. Pavlowsky, Ph.D., Thesis Committee Chair

Toby J. Dogwiler, Ph.D., Committee Member

Xiaomin Qiu, Ph.D., Committee Member

Julie Masterson, Ph.D., Dean of the Graduate College

In the interest of academic freedom and the principle of free speech, approval of this thesis indicates the format is acceptable and meets the academic criteria for the discipline as determined by the faculty that constitute the thesis committee. The content and views expressed in this thesis are those of the student-scholar and are not endorsed by Missouri State University, its Graduate College, or its employees.

ACKNOWLEDGEMENTS

I would like to thank the following people for their knowledge and support during the course of my graduate studies, firstly my thesis advisor, Dr. Robert Pavlowsky and committee members, Dr. Toby Dogwiler and Dr. Xiaomin Qiu. I would also like to thank the following people who helped conduct field work and collect data for this research, Shay Hostens, Triston Rice, Dylan King, Leah Bournival, Grace Roman, Katy Reminga, Hannah Adams, Sarah LeTarte, Kelly Rose, Miranda Jordan, and Drs. Jake Bendix and Derek Martin. Additionally, I would like to thank the faculty and staff of the Missouri State University Geography, Geology, and Planning Department who encouraged me to pursue graduate studies and provided guidance and support.

I would like to acknowledge and thank the National Science Foundation for providing funding for this research through RAPID- Impacts of an extreme flood on riparian forests and large woody debris in the Ozark Highlands, Project #1748816. In addition, I want to thank the Ozarks Environmental and Water Resources Institute, Missouri State University Graduate College, and Department of Geography, Geology and Planning for providing funding and the opportunity to work as a graduate assistant.

Thank you to all my friends and family who have encouraged and supported me throughout these last few years. I am extremely grateful for all you have done for me.

TABLE OF CONTENTS

LIST OF TABLES

LIST OF FIGURES

CHAPTER ONE: INTRODUCTION

Riparian forests grow in the transitional zone between stream and valley (Naiman and Decamps, 1997). They provide important geomorphic and ecologic functions in fluvial systems such as flood retention (Johnson et al., 2000), bank and floodplain stabilization (Hupp and Osterkamp, 1996; Tal et al., 2004), and maintenance of eco-hydrologic regime (Gran and Paola, 2001). Additionally, riparian forests filter sediments and pollutants and increase biodiversity by providing habitat (Raeker et al., 2008). Floods are a significant source of disturbance in riparian zones and often control forest structure (Bendix, 1997). Therefore, riparian forests reflect a balance between flood disturbance and recovery, where the spatial distribution of riparian vegetation is limited by the frequency, magnitude, and duration of streamflow (Hupp and Osterkamp, 1996). Given the strong relationship between flood regime and riparian forest growth, there are increasing concerns of flood risks from climate change. Climate change models around the world have found increases in the frequency of high flow events, seasonal runoff, and flow variability by season and geographic location (Chang et al., 2002; Andréasson et al., 2004). Increases in flood frequency, mean flow, and flow variability have also been modeled in the northeastern United States since the 1990s (Poff et al., 1996). Due to the potential damage that can be caused by floods, these changes in hydrology threaten riparian forests (Swanson et al., 1998; Johnson et al., 2000; Garssen et al., 2017).

It is well known that large floods can cause extreme geomorphic changes to fluvial systems through rapid channel erosion, excessive sediment transport, and debris flows (Phillips, 2002; Morche et al., 2007; Fuller, 2008; Borga et al., 2014). A 100-year flood on a wandering river in New Zealand, caused a five-fold increase in active channel width and a six-fold increase

in bar area (Fuller, 2008). A 40-year flood event in an alpine river (17 km^2) eroded more than 100,000 tons of sediment, causing large scale channel changes and sedimentation downstream (Morche et al., 2007). However, the geomorphic effects of large floods can vary. In a study on a 200-year flood in Hungry Mother Creek (17 km^2), Virginia, channel incision and bank erosion were common, however the geomorphic impacts of the flood were minimized due to the dominantly forested land use of the watershed and the timing of the flood during peak vegetation cover in the summer (Phillips, 2002).

Forest damage from flooding refers to the removal, toppling, and/or mortality of vegetation, with effects varying between lowland and highland watersheds (Swanson et al., 1998; Johnson et al., 2000; Kozlowski, 2002). Riparian vegetation damage in lowlands typically comes from relatively long periods of inundation, which reduce oxygen levels in soils, causing biomass loss and root death and decay (Kozlowski, 2002). Prolonged inundation is typical of lowland flooding in which the duration of floods can last weeks to months (Swanson et al., 1998). Garssen et al. (2017) found that in lowland flooding, flood water depth (magnitude) over the forest floor increased plant mortality and decreased plant diversity. Whereas riparian forest damage in lowland flooding mostly comes from the interaction between flood waters and soil conditions/oxygen depletion (Kozlowski et al., 2002; Garssen et al., 2017), riparian forest damage along highland streams mainly comes from mechanical damage due to floating wood collisions and high stream power which can erode substrate and topple trees (Johnson et al., 2000). Additionally, it is known that floods in mountainous landscapes are shorter in duration (hours to days) and that flood disturbance typically consists of debris flows, scoured channels, and floating woody debris (Swanson et al., 1998).

Floods can cause tree damage through direct contact with the hydraulic force of the flow and through collisions with floating wood or falling trees (Swanson et al., 1998; Johnson et al., 2000). Trees may become undercut and toppled or uprooted due to substrate failure or floating debris impacts (Swanson et al., 1998; Johnson et al., 2000). Swanson et al. (1998) observed a large (1.5 m diameter) conifer log topple adjacent riparian trees as it was transported by high streamflow. Riparian vegetation cover typically decreases during floods due to an increased active channel width (Friedman and Lee, 2002). However, after floods, riparian vegetation cover (and/or density) may increase past its initial extent due to increased space and moisture availability (Bendix, 1998; Friedman and Lee, 2002; Garssen et al., 2017). There are relatively few studies of large flood (>100-year recurrence interval) effects on riparian forests in higher relief regions, with a few exceptions (Swanson et al, 1996; Johnson et al., 2000; Friedman and Lee, 2002). This study examines the relationship between a large magnitude flood event and riparian forest response in the Ozark Highlands region of the Midwest United States.

Potential for UAV Monitoring

Aerial photographs have been used before to define flooded areas, assess damages, and identify flood susceptible areas (Klemas, 2015). Additionally, landforms, forests, and rivers have been monitored using aerial photography and photogrammetry as well (Chandler et al., 2002; Fujita et al., 2003; Everitt et al., 2010; Dandois et al., 2015; Warrick et al., 2017). Historically, aerial photography provided data that could be used to calculate changes in areal extent of vegetation (Everitt et al., 2010) and to identify canopy gaps in forests (Fujita et al., 2003). However, traditional means of acquiring aerial photographs or other imagery has limitations, such as high cost and low spatial resolution (Anderson and Gaston, 2013).

Recently, unmanned aerial vehicles (UAVs) have become capable of acquiring high-resolution images. UAVs provide cost-effective options for collecting high-resolution aerial imagery (Quilter and Anderson, 2000). Additionally, UAVs provide several other benefits compared to alternatives, UAVs can provide information about inaccessible or hard to reach areas, are non-invasive, can be used to detect and measure change, and allow for control of survey revisit periods (Quilter and Anderson, 2000; Anderson and Gaston, 2013). Recently, UAVs have been used to collect imagery for environmental assessments ranging from beach morphology surveys (Jeong et al., 2018) to monitoring stream and riparian restoration projects (Quilter and Anderson, 2000). Forest and river characteristics, including; canopy gaps, canopy heights, and landforms have been successfully measured with UAV imagery (Dandois and Ellis, 2010; Getzin et al., 2012; Zahawi et al., 2015; Watanabe and Kawahara, 2016).

Purpose and Objectives

Most studies of large woody debris and riparian tree effects from flooding in the United States have been completed outside of the Midwest, with many focusing on mountain streams in the western United States (Swanson et al., 1998; Johnson et al., 2000; Fierke and Kauffman, 2006; Wohl and Cadol, 2011). Although riparian forests provide important ecologic and geomorphic functions critical to maintaining riverine ecosystems (Raeker et al., 2008), no in-depth studies of the relationship between floods and riparian vegetation/large woody debris have been completed in the Ozark Highlands, in the Central United States. Some studies have noted that vegetation-landform relationships reflect the geomorphic stability of the channel and the role of vegetation in controlling channel form in Ozarks streams (Mckenney et al., 1995). Others have shown that the spatial distribution of large woody debris has strong spatial periodicity in

some segments of the Big River in the Ozarks (Martin et al., 2018). However, the geomorphic variables (sinuosity, meander wavelength, and gravel bar spacing) that were tested showed poor relationships with the deposition location for the large wood (Martin et al., 2018). The lack of studies on the hydraulic and geomorphic factors which control riparian forest distribution show the need for further research and understanding of riparian vegetation and large woody debris in the Ozarks.

There are increasing concern of climate change and flood effects in the Midwest and the Ozark Highlands region. Across the Midwest, annual precipitation has increased up to 20% in some locations; much of this increase comes from an increase in intensity of heavy rainfall events (Pryor et al., 2014). The increase in frequency and intensity of extreme precipitation events is expected to continue and produce more frequent floods and flood-related problems (Pryor et al., 2014). The recent increase in higher rainfall intensity events has also been observed in the Big Barren Creek watershed in the southeast Missouri Ozarks (Pavlowsky et al., 2016). Additional studies in the Ozarks have shown that the discharges of both small and large recurrence interval floods have been increasing (Foreman, 2014). Increases in extreme precipitation can cause increased erosion and sediment transport and damage in riparian ecosystems (Pryor et al., 2014). Additionally, the Ozark Highlands region in southern Missouri has also been experiencing a significant increase in annual peak discharge since the 1970s (Heimann et al., 2018).

The purpose of this study is to add to our understanding of how extreme floods and geomorphic factors affect riparian forests in the Ozark Highlands. The occurrence of an extreme flood in April 2017 provided an opportunity to assess patterns of riparian forest damage (Heimann et al., 2018). The objectives of this study are to assess the geomorphic setting and

characteristics of six study reaches in the North Fork of the White River watershed in Southern Missouri, use low altitude UAV imagery to assess forest disturbance, and evaluate the influence of hydrologic and geomorphic factors on observed patterns of forest disturbance. Geomorphic variables such as, basin slope, valley form and confinement, sinuosity, reach slope, channel morphology, bed substrate, floodplain features, and hydrology will be used to evaluate the spatial distribution forest damage. Stream power, channel planform, floodplain topography, and type of tree disturbance will be evaluated for their influence on the patterns of forest damage. The use of UAV imagery will also be compared with field measurements to assess the capabilities of UAVs in acquiring accurate quantitative data on riparian forest damage.

Benefits. This study provides analysis and evaluation of the effects of a rare flood event on riparian forests in a region generally lacking previous bio-geomorphic studies (Mckenny et al., 1995; Martin et al., 2018). The relationship between floods and flood effects is complex, with flood effects varying greatly across stream reaches and watersheds (Bendix, 1997; Swanson et al., 1998; Johnson et al., 2000). Understanding of the geomorphic and hydrologic variables that generally control flood damage is fairly well documented (Bendix, 1994; Bendix, 1998; Swanson et al., 1998; Johnson et al., 2000, Engelhardt et al., 2011), however there are few studies that specifically examine the immediate effects of the largest flood on record on riparian forests. This type of research is also important since large floods can cause billions of dollars' worth of damages to property and infrastructure (Pryor et al., 2014). Knowing the variables that control large flood effects can inform land management decisions and potentially reduce flood damage to properties and infrastructure. This study will further our understanding of the relationship between riparian forests and large floods and more broadly about the increasing risks of floods due to climate change.

Study Area

The North Fork of the White River (3,600 km^2) is located in south-central Missouri and flows south into Norfolk Lake in north-central Arkansas (Fig. 1). The majority of the watershed is in the counties of Ozark, Douglas, and Howell in Missouri (Miller and Wilkerson, 2001). The present day land use of the North Fork River watershed consists mostly of forest (62.7%) and pastureland (28.3%), with less than 4% covered by urban areas (MRLC, 2016). About 13% of the land in the North Fork River watershed is public land, mostly as part of the Mark Twain National Forest (Miller and Wilkerson, 2001). Six tributary study sites of the North Fork of the White River were examined in this study. All the sites are in western Howell County except for one, in eastern Douglas County (i.e. Indian Creek) (Fig. 1).

Geology and Soils. The North Fork River watershed generally drains horizontally bedded sandstones and dolomites of Ordovician and Mississippian age (Miller and Wilkerson, 2001). Karst features, such as sinkholes, caves, springs, and losing streams are commonly found throughout the watershed (Miller and Wilkerson, 2001). Sinkholes are have been mapped in all six of the watersheds in this study except at Lick Branch, which has the smallest drainage area (4.5 km^2) (Duley et al., 2015). Steep ridges and high bluffs are characteristic of Ozarks stream systems with up to 200 m in relief (Jacobson and Primm, 1997). High relief can contribute to increased runoff rates, flood energy, and riparian damage. Upland soils in the North Fork River watershed are primarily formed in the weathered residuum of limestone and dolomite bedrock and overlying thin loess deposits, when present (Miller and Wilkerson, 2001). Upland soils formed in Pleistocene glacial loess deposits make up 11% of the combined areas of the six tributary watersheds studied (USDA, 2005; USDA, 2006). Soils range from deep to shallow, moderately well drained to excessively well drained, are loamy and contain large amounts of

chert fragments in the subsoil (Miller and Wilkerson, 2001). Chert fragments in soils of the North Fork River watershed vary from 0-85% (USDA, 2005; USDA, 2006). Depth to bedrock ranges from 0.5 m to greater than 1.5 m (USDA, 2005; USDA, 2006).

Ozark's Forest History. The Ozark Highlands have a long history of forest exploitation and management within the Mark Twain National Forest. In the 1850s, relatively large areas of shortleaf pine forest (230 – 340 km^2) were logged along tributaries of the North Fork River in Ozark, Douglas, and Howell County (Sauer, 1920). These "pineries" yielded logs 24-27 m in length and up to 1.2 m in diameter (Sauer, 1920). Between 1880 and 1920, pine logging and timber production peaked in the Ozarks, with oak and other hardwoods harvested after pine was depleted (Jacobson and Gran, 1999). Logging and agricultural practices disturbed Ozarks streams by increasing runoff, tributary stream erosion, and releasing large amounts of gravel to streams causing instability, bank erosion, and habitat degradation (Jacobson and Gran, 1999; Martin and Pavlowsky, 2011). These disturbance reaches tend to intensify flood effects on riparian forests because they are areas of channel instability with higher rates of erosion and sedimentation (Mckenney et al., 1995). In the 1930s, land management began in the North Fork River watershed with the creation of the Mark Twain National Forest System (Miller and Wilkerson, 2001).

Ozark's Riparian Forest Composition. Pre-settlement forest composition of the Ozarks and the North Fork River watershed was mostly oak-pine forest (Sauer, 1920; Raeker et al., 2008). The current composition is now mostly oak-hickory with some oak-pine forest (Raeker et al., 2008; Lyons and Sager, 1998). The dominant canopy species are shortleaf pine, oak, and hickory (Stambaugh et al., 2002). The five most common canopy species inventoried along several transects during this study were White Oak (*Quercus alba*) (43%), Shortleaf Pine (*Pinus*

echinata) (10%), American Sycamore (*Platanus occidentalis*) (9%), other oak species (9%), and White Ash (*Fraxinus americana*) (7%). All of these species (except the shortleaf pine) have been used to restore riparian areas in the Ozarks (Steele et al., 2013).

Climate. The average annual precipitation in the North Fork River watershed was 110 cm for the period of 1946 to 1995, with the maximum annual precipitation of 166 cm and a minimum of 52 cm (Miller and Wilkerson, 2001). The annual precipitation in nearby West Plains, MO in 2018 was 132 cm (MRCC, 2019). The spring and early summer months of April, May, and June typically receive the most precipitation, while December, January, and February receive the least (Miller and Wilkerson, 2001). Average temperatures in the Midwest, have been increasing by 0.06 degrees Celsius per year from 1900-2010 (Andresen et al., 2012). Additionally, average annual precipitation has been increasing over time in the Midwest (Andresen et al., 2012) and in the North Fork River watershed (Miller and Wilkerson, 2001). In the North Fork River watershed, average annual precipitation has increased 6.5 cm when comparing the years 1946-1970 and 1971-1995 (Miller and Wilkerson, 2001). The frequency of daily precipitation events greater than two inches has also increased across the Midwest from 1985 to 2014 (Heimann et al., 2018).

Occurrence of a >500-year Flood. On April 28-April 30, 2017, a large storm system moved across the Midwest recording heavy rainfall across southern Missouri (US Department of Commerce, 2017). In the counties of Ozark, Douglas, and Howell (including the North Fork River watershed) over a period of 48 hours, 20-30 centimeters of rain fell (Fig. 2) (US Department of Commerce, 2017). This led to severe flooding on the North Fork of the White River, which destroyed buildings, roads, and bridges. Twenty-one rivers in the Midwest had record-breaking peak discharges, including fourteen rivers in southern Missouri and the North

Fork River (Heimann et al., 2018; Erdman, 2017). The USGS, recorded the peak discharge of the flood event at the North Fork River near Tecumseh, Missouri (USGS stream-gage number 07057500) at 189,000 cfs, with a peak stage of approximately 13 m and a recurrence interval of greater than 500 years (Heimann et al., 2018).

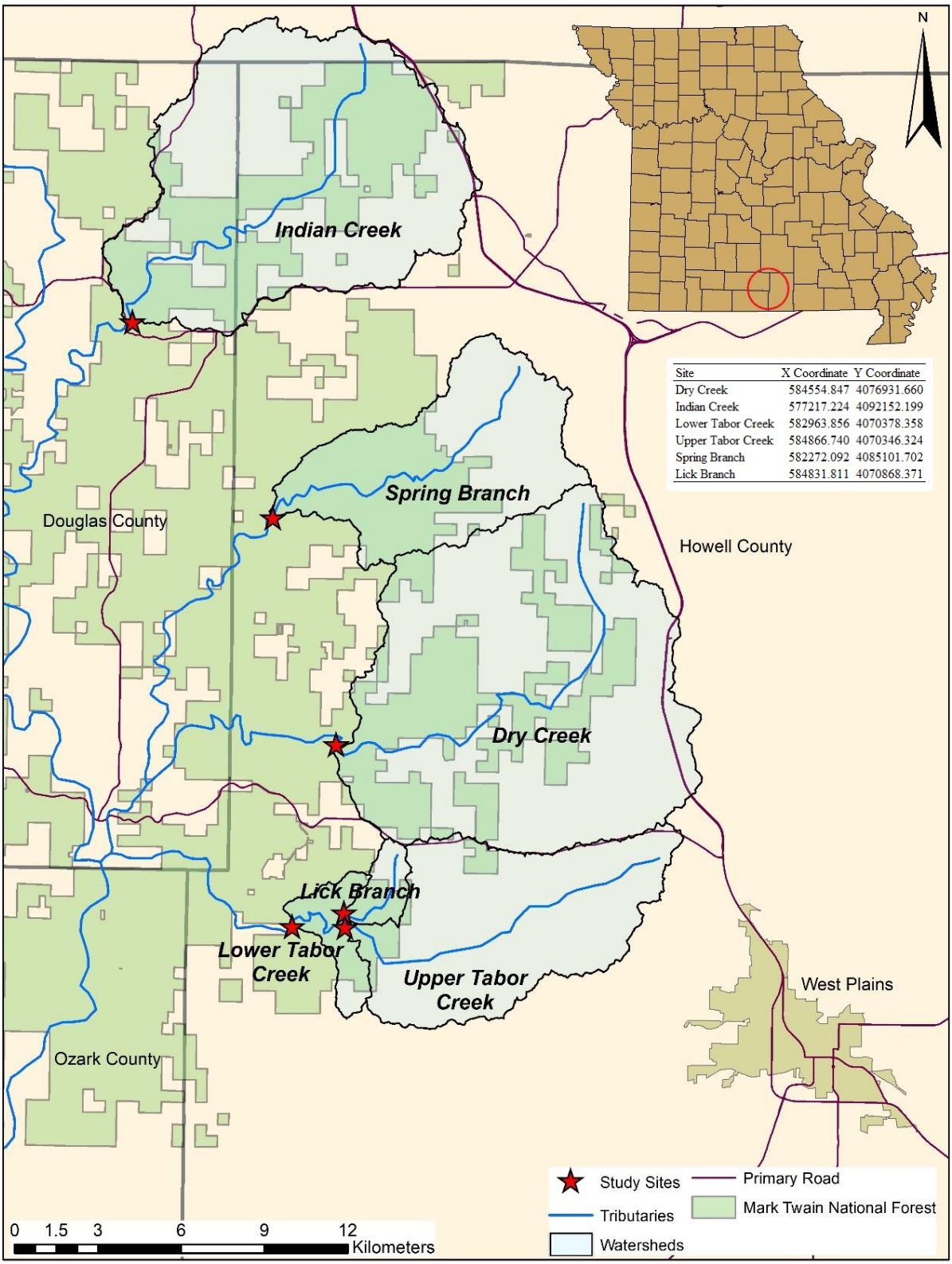

Site	X Coordinate	Y Coordinate
Dry Creek	584554.847	4076931.660
Indian Creek	577217.224	4092152.199
Lower Tabor Creek	582963.856	4070378.358
Upper Tabor Creek	584866.740	4070346.324
Spring Branch	582272.092	4085101.702
Lick Branch	584831.811	4070868.371

Fig. 1. Location of the Six Study Sites

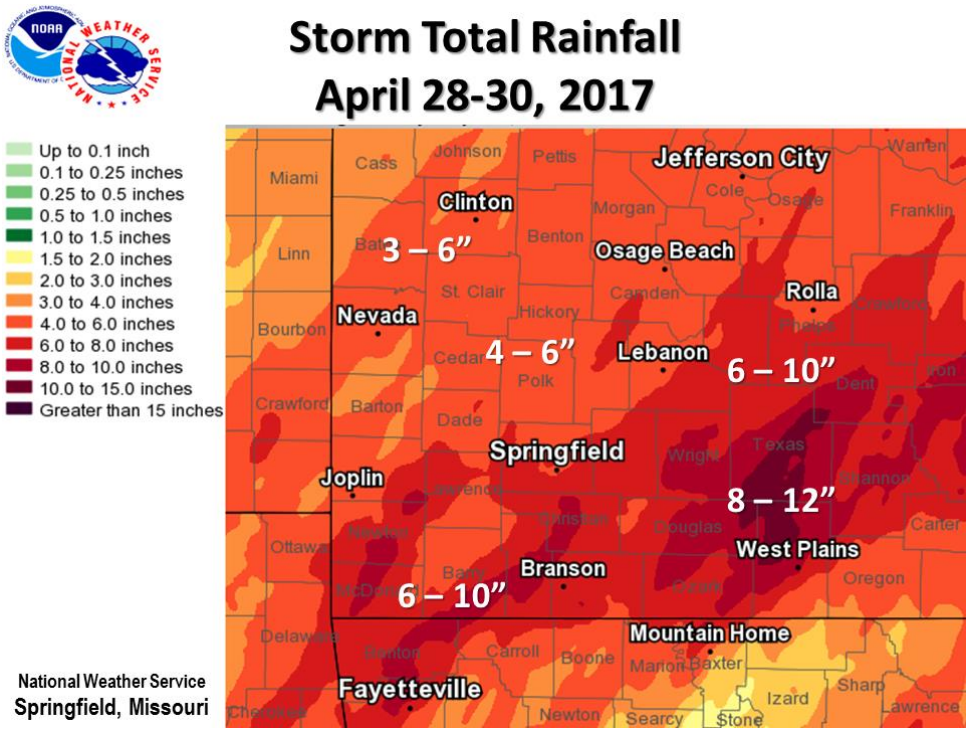

Fig. 2. Rainfall Map of Missouri Ozarks During April Storm Event, from the National Weather Service

CHAPTER TWO: RIPARIAN FOREST DAMAGE AND PATTERNS

The relationship between flooding and riparian forest damage is poorly understood in the Missouri Ozarks. However, previous work on riparian forest damage by floods conducted outside of the Midwest provides information on potential geomorphic factors that may contribute to tree damage. Valley confinement, channel sinuosity, substrate erosion, and stream power have been reported to be significant variables in maximizing the geomorphic effectiveness of floods and flood effects on riparian vegetation (Bendix, 1998; Swanson et al., 1998; Bendix and Hupp, 2000; Johnson et al., 2000). The purpose of this chapter is to assess the post-flood geomorphic setting and riparian forest damage along six tributary streams of the North Fork of the White River in Missouri (Fig. 1). Specific objectives include: Geomorphic mapping of each sampling reach; Assessment of riparian tree damage using UAV imagery and field ground-truthing; and; Analysis of the relationship between geomorphic variables and tree damage by size, location, basal area, and volume.

Hydro-Geomorphic Factors of Riparian Forest Damage

Valley Confinement. Valley confinement is defined by the ratio between valley width (maximum flood-prone area) and bank-full channel width (Nagel et al., 2014). Confined channels in mountain streams tend to generate more damage to riparian forests due to the constriction of high energy flows compared to unconfined areas where there is greater floodplain area and/or secondary channels (Swanson et al., 1998; Johnson et al., 2000). Additionally, Wohl and Cadol (2011) found that in confined channels in the Colorado Front Range, wood pieces were highly aggregated and had a tendency to form jams. Nagel et al. (2014) classified ratios of

<3.8 as confined channels and ratios >3.8 as unconfined channels. However, others define confinement as, “the percentage of length of the stream or river channel segment that abuts a confining margin on either bank”, such as a valley wall or anthropogenic margin (Fryirs et al., 2016).

Sinuosity. Sinuosity measures bends in the stream channel and is defined as the length of the channel reach along the thalweg divided by the straight-line distance between the start and endpoint of the reach (Leopold and Wolman, 1957). Forest damage is typically increased at channel bends compared to straight sections. Bends in the stream channel allow for overbank flows to directly enter riparian forests and maximize bank/substrate erosion rates and thus locally increasing the supply and quantity of wood that is stored (Nakamura and Swanson, 1994; Gurnell et al., 2002). Additionally, bends in the stream channel maximize erosion rates (Leopold and Wolman 1957; Hupp and Osterkamp, 1996) and contribute to further damage of riparian vegetation by undercutting vegetation on stream banks (Johnson et al., 2000). Fuller (2007) found that in the Kiwitea drainage basin in New Zealand, confinement of flood flows at bends in the stream enhanced stream power and thus the tendency for major geomorphic adjustment. Additionally, jams of large woody debris have been found to form on the outside bends of channels during over-bank flooding (Nakamua and Swanson, 1994; Gurnell et al., 2002).

Secondary channels/chutes influence the accumulation and storage of large wood debris (riparian forest damage) (Nakamura and Swanson, 1994). Chutes develop on floodplains during overbank flows when there is enough energy to erode floodplain sediments (Harrison et al., 2015). Chutes typically form along sinuous reaches, in areas downstream from bends in the channel (Harrison et al., 2015). In this study, chutes were located downstream from channel bends on floodplains (Fig. 3a, 3b, 3c) and within backswamp positions along valley margins

(Fig. 3c and 3d). Deposition locations for large woody debris are influenced by chute locations (Nakamura and Swanson, 1994). Storage of large woody debris typically occurs at the entrance of and within the secondary channels/chutes (Nakamura and Swanson, 1994). Large woody debris typically accumulates on the outer bends of secondary channels/chutes, just as it does on the main channel (Gurnell et al., 2002). Nakamura and Swanson (1994) found that reaches with chutes had almost twice the wood debris density of single channel reaches. Since overbank flows that create chutes are erosive (Harrison et al., 2015), it is logical to assume that where chutes occur and direct flood waters may have more riparian forest damage due to erosion and impacts of large woody debris (Johnson et al., 2000). Lick Branch and Upper Tabor Creek were the only sites that did not have chutes in the sample reach (Fig. 3e and 3f).

Substrate. Vegetation can be damaged by the erosion of sediment deposits on landforms in which they are growing (Bendix and Hupp, 2000). Thus areas where the substrate is easily erodible and mobilized by floods have greater potential for riparian forest flood damage. High energy streamflow can erode streambanks removing the soil where the roots of trees are located, thus potentially toppling, killing, removing and/or severely damage trees (Johnson et al., 2000; Hupp and Bornette, 2005). Streambank erosion supplies wood to streams by mobilizing large woody debris on the banks and undercutting standing vegetation (Murphy and Koski, 1989; (Piégay et al., 1998; Johnson et al., 2000). In a study on the flood effects of a 40-year flood event, Morche et al. (2007) found that large woody debris in the stream was mainly supplied by eroded streambanks. Bendix (1998) suggests that even in flood resistant species, substrate erosion may be a more important factor of flood damage than the flood resistant attributes of the species.

Only three different soil series are mapped for the sample reaches in this study, with most of the sites covered by only one soil series (USDA, 2005; USDA, 2006) (Table 1). Given that the soil properties are very similar among the series, potential rates of substrate erosion may generally not vary much among these sites (Table 1). Thus this variable is probably not useful in sorting out differences in substrate resistance to flood damage at the site-scale used in this study. Alluvial soil series at the sites range from gravelly sandy loam to silt loam and contain relatively large percentages of gravel (USDA, 2005; USDA, 2006) (Table 1).

Stream Power. In forested mountain streams, Johnson et al. (2000) found that riparian vegetation interactions with geomorphic processes were increased due to high stream power, sediment transport, and large quantities of wood. Stream power can be calculated as cross-sectional (W/m) and mean (W/m^2). Cross-sectional stream power refers to the sediment transport capacity of the flow and mean stream power refers to the transport competency of the flow (Bull, 1979; Lecce, 1997). Cross-sectional stream power is calculated using the specific weight of the fluid, discharge, and slope (Bull, 1979; Lecce, 1997). Mean stream power is calculated using the specific weight of fluid, the hydraulic radius, flow velocity, and slope (Lecce, 1997). Both measurements of stream power relate to the geomorphic work that can be achieved by the streamflow. However, mean stream power has been used before to test the relationship between flood damage and riparian species distribution and is a suitable measure of the possible flood damage to riparian vegetation (Bendix, 1999).

Stream power indicates the force of the water acting on the vegetation as well as the impacts of sediment and debris encountering vegetation and potentially damaging it (Bendix, 1999). Channel areas where stream power is relatively high are more sensitive to floods since there is more energy available to do geomorphic work (Engelhardt et al., 2011). Increased stream

gradient typically increases stream power (Bendix, 1997) and reaches generating greater stream power during large floods have more tree damage and decreased vegetation cover (Bendix, 1994; Engelhardt et al., 2011). Additionally, stream power typically increases downstream with increases in discharge (Graf, 1983). However, Lecce (1997) showed that cross-sectional and mean stream power peaked in drainage areas between 10-100 km^2 in the Blue River watershed, in southwestern Wisconsin. The geology and soils of southwestern Wisconsin are similar to the North Fork River watershed, therefore this finding suggests that reaches with relatively high discharge in intermediate drainage areas may produce the greatest rates of riparian forest damage in the Ozark Highlands.

Study Area

Six sites on tributaries of the North Fork River were selected based on the location of the highest rainfall amounts, Mark Twain National Forest access, and sampling across variable drainage area (Fig. 1). The six sites selected for analysis and drainage area are as follows: Dry Creek (124.2 km^2), Indian Creek (101.6 km^2), Lower Tabor Creek (65.4 km^2), Upper Tabor Creek (54.0 km^2), Spring Branch (49.1 km^2), and Lick Branch (4.5 km^2) (Table 2). Forested land use is the majority land use at each site except for Upper Tabor Creek, which has agriculture as the primary land use (Table 2). A total of three alluvial soils series are present at the sites, with one soil series covering all of the valley bottom at all the sites except at Dry Creek (USDA, 2005; USDA, 2006) (Table 1). The alluvial soil series range from young and thin entisols on floodplains to more developed alfisols on terraces and alluvial fans (USDA, 2005; USDA, 2006). The alluvial soils at each site range from 10-96% sand and 0-85% gravel (USDA, 2005; USDA,

2006). Surface soil was typically less gravelly sandy loams and silt loams, while the subsoil contained more gravelly loamy sands and clays (USDA, 2005; USDA, 2006) (Table 1).

Methods

Field Methods. Geomorphic assessments were completed at each site in September, 2017. Sample reaches were divided by 11 transects, each spaced at approximately two bankfull channel widths apart. Locations of geomorphic features (channel, floodplain, chute, terrace, and tributaries) were recorded using Trimble GPS units. High water marks were also noted, and were used estimate the flood level (Morche et al., 2007). Pebble counts were completed at riffles, glides, and bars at each site in order to determine the sediment distribution of channel deposits. Pebble counts were conducted perpendicular to the stream at riffles generally following procedures outlined by Wolman (1954). Blind sampling of the sediment was achieved by measuring the first piece of sediment that the index finger touched while not looking at the ground. The b-axis of the sediment was then measured with a gravelometer and recorded. This process was continued across the stream until reaching the other bank, and then continued in a grid pattern across the riffle. Typically five transects were sampled across the channel unit at 2 m spacing within a specific channel unit to collect 30 samples.

Topographic surveys using an auto-level and pulled tapeline were completed at one to two valley cross-sections at each sampling reach in September of 2018 to measure channel dimensions, floodplain and terrace elevation, and landform locations (Rosgen, 1996). Longitudinal profiles were completed to calculate reach slopes and channel bedforms (Rosgen, 1996). The slopes and valley/channel characteristics were then used to model flows and estimate discharge and stream power.

Field tallies of riparian trees and their attributes were conducted in April, 2019 at each site along the same cross-valley transects surveyed in September, 2018. The transect was used as a baseline for a 5 m wide sampling zone of all damaged and standing riparian trees (Katz et al., 2005). Standing tree diameter was recorded in order to calculate basal area per the sampling zone. Damaged trees were recorded as toppled or uprooted (Everham and Brokaw, 1996; Swanson et al., 1998; Johnson et al., 2000). Damaged tree length and diameter were recorded in order to estimate the volumes of the wood in the zone and to compare with measurements derived from the UAV imagery. Additionally, orientation and some species identification data were recorded.

Geospatial Data Collection and Analysis Methods. For this study, a combination of UAV flight plans were used to generate orthophotos and Digital Surface Models (DSMs) of each site. UAV imagery was obtained once during the leaf-on season (September 2017) and once during the leaf-off season (March 2018). The UAV imagery and GPS data points of geomorphic features were uploaded into ArcMap and used to create geomorphic maps and show riparian forest damage. The use of aerial photographs and ArcGIS to assess forest damage has been used before and is helpful in assessing forest damage (Kupfer et al., 2008). Using the UAV imagery as a base-map, shapefiles were created to digitize the locations of bankfull channel boundaries, floodplain boundaries, chutes, terraces, and tributaries. Landforms were also identified with the help of alluvial soil data (USDA, 2005; USDA, 2006) and DEMs (Martin and Pavlowsky, 2011). Additionally, vegetation lines on the banks of the channels were used to help delineate the channel (Vanlooy and Martin, 2005).

Damaged and standing riparian trees were identified and assessed using the UAV imagery. Tree condition in forest surveys is usually considered as standing or toppled (Swanson

et al., 1998; Johnson et al., 2000) but can be further classified as uprooted or broken (Everham and Brokaw, 1996). Tree toppling is an important forest damage attribute because a 45 degree lean has been found to be a critical point for survival (Brewer and Linnartz, 1973). The angle of leaning trees could not be measured in the UAV imagery, so toppled trees were identified in the UAV imagery by using the shadows of the trees and comparing them to the angles of shadows of adjacent standing trees. Uprooted riparian trees were identified by looking for exposed rootwads or tree stems that were broken/transported. Damaged riparian trees were given the following attributes: condition (uprooted or toppled), azimuth (from rootwad to crown), jam present (yes or no), length, diameter, and volume. Azimuth was estimated to see if the damaged tree orientation aligned with the adjacent streamflow. Length of the damaged trees was measured from the top of the rootwad to the base of the crown. Diameter was measured at the approximate center of the visible portion of the tree. Disturbed forest sites also classify damage by the complete removal of trees (Johnson et al., 2000), the number or areal percentage downed (Kupfer et al., 2008), and the remaining or removed canopy cover (Everham and Brokaw, 1996; Stephens et al., 2008). For this study canopy loss was calculated using the leaf-on (September 2017) UAV imagery and DSM and comparing it with 2016 leaf-on NAIP imagery.

Channel Hydraulics and Hydrology. Peak discharge for 2-500 year RI floods were estimated using a published regional regression equation with drainage area and basin slope as independent variables (Alexander and Wilson, 1995). Basin slope is calculated as the difference in elevation at points 10 and 85 percent of the distance along the main channel from the lowest end of the stream to the basin divide, divided by the distance between the two points (Alexander and Wilson, 1995). Basin slope was calculated using a 10 m resolution DEM. Intelisolve Hydraflow Express (2006) software was used to model flows based on observed high water

marks and estimated discharges for certain recurrence interval floods through the surveyed cross-sections and compared to one another. Manning's n roughness coefficient values were determined for each cross-section using Chow (1959). Manning's roughness coefficients ranged from 0.04 -0.06 across channels and bars, 0.1 – 0.12 across floodplains and terraces, 0.06 – 0.085 across valley floor features with riparian forest damage, 0.04 – 0.10 across chutes, varying with the amount of forest damage.

Geomorphic Channel Analysis. Landform distribution was determined using the surveyed valley cross-sections, the UAV DSM imagery, and flow stages modeled through Intelisolve Hydraflow Express (2006). The active channel was defined as the bankfull channel with the capacity to contain the 1.5 – 2 year RI flood. Floodplain features started from the bankfull elevation and ended either at the valley margin or where terrace features began. Terrace features where marked as higher elevations than floodplains, usually greater than the 10-year RI flood. Sinuosity was calculated as the length of the channel along the thalweg divided by the straight-line distance between the start and endpoint of the reaches (Leopold and Wolman, 1957). Confinement ratio was calculated as the width of the valley divided by the width of the bankfull channel, this was calculated at each transect and then averaged by site (Nagel et al., 2014).

Cross-sectional stream power and mean stream power were calculated for flows at the predicted 500-year flood discharge (using Alexander and Wilson, 1995). Cross-sectional stream power (W/m) was calculated for each site using $\Omega = \gamma QS$ (Bull, 1979; Lecce, 1997), where γ is the specific weight of the fluid, 9,810 N/m^3 (the density of water (1000 kg/m^3) and the acceleration due to gravity (9.81 m/s^2) and where Q is discharge (m^3/s) and S is slope (m) (Lecce, 1997). Mean stream power (W/m^2) was calculated using as $\omega = \gamma RSV$, where R is the

hydraulic radius (m), V is the flow velocity (m/s), and S is slope (m) (Lecce 1997). Although the density of water is likely to be greater during floods (Bendix, 1999), the water density value makes little difference to the end result (Costa, 1983). Once sinuosity, confinement, stream power, and sediment distribution were calculated, regression analysis was performed to see how these variables account for the variance in riparian forest flood damage.

Forest Damage Results and Discussion

Channel and Valley Characteristics. In general, sampling sites were located in watersheds containing primarily forested land-use (Table 2). This was the case at all of the sites except at Upper Tabor Creek in which 50% of the watershed was used for agriculture (Table 2). Additionally, Upper Tabor Creek contained the least amount of land (7%) within the Mark Twain National Forest system, while Lick Branch contained the most (62%) (Table 2). Basin slope, calculated using the method of Alexander and Wilson (1995) ranged from 0.005 m/m at Upper Tabor Creek to 0.013 m/m at Lower Tabor Creek and Lick Branch (Table 2). Differences in land-use and basin slope may influence forest damage throughout watersheds. Increased slope typically increases stream power (Bendix, 1997). Land-use causing soil disturbance or adding impervious area can reduce roughness and increase runoff rates and sediment loads (Shepherd et al., 2010).

Valley confinement and sinuosity were greatest at Lower Tabor Creek. Average valley confinement ranged from 1.2 at Lower Tabor Creek and to 5.8 at Dry Creek and Spring Branch (Table 3). However, reach-scale variability in valley confinement was greatest at Dry Creek (CV% = 43%) and lowest at Lick Branch (CV% = 20%) (n = 11) (Table 3). The range in sinuosity values was relatively narrow (1.02 to 1.16) with the exception of Lower Tabor Creek

(1.75) (Table 3). Valley confinement and sinuosity have previously been reported to be significant factors in affecting riparian forest damage (Swanson et al., 1998; Johnson et al., 2000), thus suggesting that forest damage might be higher at Lower Tabor Creek.

Active channel width was lowest at Lick Branch (13 m) and highest at Lower Tabor Creek (48 m) (Table 3). Variability (CV%) in active channel width ranged from 10% at Upper Tabor Creek to 48% at Spring Branch (Table 3). Valley width ranged from 59 m at Lick Branch to 128 m at Spring Branch (Table 3). Variability in valley width was greatest at Lower Tabor Creek (45%) and lowest at Lick Branch (5%) (Table 3).

In general, sediment distribution in riffle channel units varied across the sites (Table 3). Median sediment size (D50) ranged from fine gravel (5 mm) at Spring Branch to coarse gravel (32 mm) at Lick Branch (Table 3) (Rosgen, 1996). Average max clast size ranged from medium cobble (108 mm) at Spring Branch to small boulder (512 mm) at Dry Creek (Table 3) (Rosgen, 1996). Pebble counts recorded in the stream channel may be better related to channel slope variables and not forest floor flood resistance. However, larger sediment, such as large boulders, in the channel, may obstruct flow, resist erosion, or trap large woody debris.

Relative landform area varied among sites with chutes typically covering the least amount of area, varying from not present in the surveyed reach area at Lick Branch and Upper Tabor Creek to 9-14% at Spring Branch, Lower Tabor Creek, and Dry Creek (Table 4; Fig. 3a - 3f). Floodplains and terraces typically covered the most valley floor area, ranging from 37% at Lick Branch to 73% at Spring Branch (Table 4; Fig. 3a-3f). Additionally, the active channel at Upper Tabor Creek and Lick Branch exhibited more of a multi-threaded planform whereas the other sites, were primarily single channel types. No single landform covered more than 63% of any site (i.e., active channel at Lick Branch) (Table 4).

Stream Power Calculations. Mean and cross-sectional stream power, calculated at the 500-year discharge, was greatest at Lower Tabor Creek (847 W/m^2 and 77,877 W/m, respectively) (Table 5). Mean 500-year stream power was lowest at Upper Tabor Creek (207 W/m^2) (Table 5). Cross-sectional 500-year stream power was lowest at Lick Branch (9,748 W/m) (Table 5). Based on these results and previous studies of forest damage Lower Tabor Creek was expected to have the greatest quantity of forest damage because of high stream power, valley confinement, and sinuosity. Lick Branch was expected to have the least damage due to lower stream power, sinuosity, and confinement.

At all the sites the average height of the observed high water mark was at or above the 500-year flood stage (Table 5). Heights of the high water marks were typically 1-2 m above the flood stage of the calculated 500-year flood peak (Table 5). The differences in flood stage depth could be as a result of scarring from branches extending above the water surface, creating high water marks above the actual depth of the water. However, at Lower Tabor Creek and Upper Tabor Creek the high water marks indicated a flood stage 3 - 4 m above the 500-year flood stage (Table 5). However, when only looking at high water marks from debris flow lines and not from tree scarring, high water marks at Upper Tabor Creek and Lower Tabor Creek were less than 2 m above the 500-year flood stage. Higher flows may also have been observed at these sites due to their drainage areas being in higher rainfall intensity areas (Fig. 2). The 500-year flood discharge was used to estimate the 500-year stream power.

Canopy Loss. Pre-flood canopy cover reflects stream processes and was typically lowest over the active channel (0-16%) and greatest over floodplains, terraces, and chutes (Table 6). Pre-flood canopy cover at each of the sites was typically high, with 81-100% of the site covered (Table 6). Canopy loss due to the flood was greatest at Lower Tabor Creek in which 63% of the

canopy cover was removed and lowest at Lick Branch and Spring Branch in which only 7-8% of the canopy cover was removed (Table 6). At Dry Creek, Indian Creek, and Upper Tabor Creek canopy loss was about 30% (Table 6). Canopy loss was greatest over the active channel at Spring Branch (48%), Upper Tabor Creek (97%), and Lick Branch (84%), and greatest over floodplains at Lower Tabor Creek (47%) and Indian Creek (48%) (Table 6). Canopy loss over terraces was greatest at Dry Creek with 50% canopy loss (Table 6). Thus canopy loss was typically greatest in the areas closest to deepest and fastest moving flood flows, near the main channel thalweg. However, canopy loss over terraces may result from adjacent chutes directing high velocity flows into the higher elevation forested areas on the valley floor.

Number and Size of Tree Damage. The number of standing trees increased with increasing sample area. Dry Creek had the most standing trees remaining on the valley bottom (266) and Lick Branch had the least amount of standing trees (73) (Table 7; Fig. 4). The number of standing trees was greatest on floodplain and terrace features at all the sites, except Lick Branch (Table 7). Chutes typically had the least amount of standing trees (Table 7). Excluding chutes, which composed the smallest area at all the sites (Table 4), the active channel typically had the least amount of standing trees (Table 7). At Upper Tabor Creek and Lick Branch, the sites without chutes, the least amount of standing trees were present on floodplains and terraces (Table 7). The amount of standing trees on terraces at Upper Tabor Creek was likely low due to the relatively small amount of area that terraces occupied (Table 4).

At each site, damaged tree diameter varied little among landform location, typically by only a few centimeters (Table 7). Average diameter at four of the six sites, including, Dry Creek (0.21 m), Lower Tabor Creek (0.19 m), Upper Tabor Creek (0.17 m), and Lick Branch (0.15 m) was largest in the active channel, while the largest diameter at Indian Creek (0.24 m) and Spring

Branch was in chutes and on terraces, respectively (Table 7). Average damaged tree length varied across landforms by a few meters and was greatest in the active channel at Indian Creek (11.9 m), Upper Tabor Creek (8.5 m), and Spring Branch (11.7 m) and on floodplains at Dry Creek (9.1 m), Lower Tabor Creek (8.9 m), and Lick Branch (5.8 m) (Table 7). Larger trees may have been found in the active channel due to proximity to higher energy flows which could topple trees through bank erosion and collisions with mobilized floating large woody debris.

Volume of Damaged Trees. Total damaged tree volume was greatest at Lower Tabor Creek (112.3 m^3) and lowest at Lick Branch (1.4 m^3) (Table 7). Damaged tree volume was typically greatest on terraces and floodplains. However, Upper Tabor Creek (29.9 m^3) and Lick Branch (0.9 m^3) had the greatest damaged tree volume in the active channel (Table 7). Damaged tree volume per hectare increased with increasing drainage area (Table 7; Fig.5). Damaged tree volume per hectare was greatest at Dry Creek (27.4 m^3/ha) and smallest at Lick Branch (5.2 m^3/ha) (Table 7). Damaged tree volume per hectare by landform showed positive relationships with drainage area, for most of the landforms (Fig. 6a-6d). The highest damaged tree volume per hectare occurred in the active channel at Upper Tabor Creek, Spring Branch, and Lick Branch (Table 7). Damaged tree volume per hectare at Indian Creek and Lower Tabor Creek was highest on floodplains and highest in chutes at Dry Creek (Table 7). This shows that damaged tree volume per hectare was typically greatest on landforms in close proximity to higher energy flows. However, vegetation damage on higher elevation landforms may be explained by the distribution of the flood resistant nature of riparian species across the valley bottom. Typically riparian species that grow on higher elevation landforms (terraces), that are less flood prone, are the least adapted for withstanding flooding (Harris, 1987).

Type and Orientation of Damaged Trees. At each site, damaged trees were typically uprooted (90%). The number of toppled trees was greatest at Dry Creek (46) and lowest at Spring Branch and Lick Branch in which there were no toppled trees. Distribution of toppled trees varied across landforms and did not show a clear pattern. Damaged tree patterns on fluvial landforms generally align with the direction of the probable streamflow (Fig. 3a-3f). Additionally, when damaged trees did not align with the flow direction of the main channel, many aligned with secondary channels/chutes flow direction (Fig. 3a-3d). Trees that either aligned with the probable main channel streamflow and/or chute flow made up 89% of the damaged trees. Trees that did not align with the streamflow were typically on higher terraces (55%) or snagged on trees or jams of debris (32%) (Fig. 3a-3f).

Riparian trees/large woody debris accumulated at the entrance of and within chutes (Fig. 3a-3d), similar to results found by Nakamura and Swanson (1994). The majority of damaged trees were not in jams (95%), similar to results found by Morche et al. (2007). At the Spring Branch and Indian Creek sites, jams occurred between the active channel and chutes on floodplains (Fig. 3c and 3a). At Lower Tabor Creek and Indian Creek jams occurred on the outside of channel bends (Fig. 3b and 3a), similar to results found by Gurnell et al. (2002).

Tree Tally Transect Versus UAV Results. Basal area of standing trees, recorded within the 5 m wide sampling transects was highest at Lick Branch transect 1 (68.5 m^2/ha) and lowest at Lick Branch transect 10 (2.5 m^2/ha) (Table 8). Previous forest studies conducted in the Ozarks have shown that basal area (of all species) range from 0 - 46 m^2/ha with an average basal area of 14 m^2/ha (Blizzard et al., 2007). In the 5 m wide sampling areas of this study, basal area ranged from 2.5 - 68.5 m^2/ha, with an average basal area of 23 m^2/ha (Table 8). However, excluding Lick Branch, which had the largest (68.5 m^2/ha) and smallest (2.5 m^2/ha) basal areas, the range

of basal areas was from 4.4 - 29.5 m^2/ha and the average was 16 m^2/ha (Table 8). This shows that the sampling transects in this study generally remained within known ranges of basal areas in the Ozarks.

Wood volume that was stored in the 5 m wide sampling zone was greatest at Spring Branch transect 5 (4.89 m^3) and smallest at Lick Branch transect 1 and 10 (0 m^3) (Table 8). Excluding transects without any stored wood (Lick Branch transects 1 and 10) Spring Branch transect 7 had the least amount of stored wood (0.58 m^3) (Table 8). Basal area and stored wood volume were inversely related, high basal area of standing trees corresponded with low stored wood volume.

When comparing the field and UAV measurements of wood volume storage in the 5 m wide sampling zone, the relationship was statistically significant ($R^2 = 0.91$, $p < 0.01$) (Fig. 7). Generally the UAV underestimated the volume of wood in the 5 m zone. This result indicates that UAV imagery can be used to quantify volumes of forest damage. However, further work needs to be done in order to identify the limitations of the UAV imagery and GIS methods in quantifying damaged tree volume.

Geomorphic Relationships with Forest Damage. Mean and cross-sectional 500-year stream power explained the greatest amount of variance in canopy loss and total damaged tree volume, typically as stream power increased so did forest damage (Fig. 8a, 8b, 9a, 9b). Mean 500-year stream power accounted for 70% of the variance in canopy loss and 67% of the variance in total damaged tree volume and was statistically significant in both cases (Fig. 8a and 8b). Mean 500-year stream power accounted for less than 20% of the variance in damaged tree volume per hectare ($p = 0.39$). Cross-sectional stream power accounted for 90% of the variance in total damaged tree volume and 73% of the variance in canopy loss and was statistically

significant in both cases (Fig. 9a and 9b). Cross-sectional 500-year stream power also explained for 48% of the variance in damaged tree volume per hectare (p-value = 0.13).

Pearson correlation analysis was used to understand the relationships between forest damage and hydrologic/morphologic variables (Table 9). Typically the best correlations between forest damage and the hydrologic/geomorphic factors occurred on floodplains and in chutes and with stream power or drainage area (Table 9). The active channel showed the lowest correlations with the variables and forest damage and showed significant correlations between forest damage and stream power, drainage area, and confinement (Table 9). Sinuosity and confinement generally did not correlate significantly with total forest damage, but were related to the damage across some of the landforms (Table 9). Further analysis showed that channel sinuosity was not a statistically significant indicator of total forest damage (i.e., volume, volume per hectare, and canopy loss) (Fig. 10). The weak positive relationships were weighted heavily by the Lower Tabor Creek sinuosity value, thus the sample size (n=6) was too small to show the relationship with forest damage. Similarly, the small sample size of this study could also not provide conclusive results of the relationship between valley confinement and forest damage (Fig. 11). Median sediment size (D50) and reach slope did not have any significant correlations with any of the forest damage across all landforms.

Correlation analysis among the geomorphic variables showed the highest correlations with mean stream power (Table 10). Basin slope, sinuosity, confinement, and median sediment size had relatively high correlations with stream power (Table 10). This indicates that mean stream power reflects the combined effects of several geomorphic forcing variables, making it a good candidate as a key variable for assessing and predicting forest damage.

Conclusions

This study examined the effects of a 500 year flood on riparian forests in the Missouri Ozarks (Heimann et al., 2018). Patterns and distribution of riparian forest damage were identified using high-resolution UAV imagery. Hydrologic and morphologic variables identified through field surveys were then used to explain the variability in riparian forest damage. There are six key findings in this study:

1. **Patterns of forest damage from this 500-year flood reveal similar results to previous studies conducted outside of the Midwest.** Generally, damaged trees were found to align with the probable streamflow (89%) and were not in jams (95%). Accumulation of damaged trees occurred on the outside of channel bends and within chutes;
2. **Canopy loss tended to increase with drainage area.** Canopy loss varied across the valley-bottom landforms, but was generally greatest closest to the active channel reflecting both flood processes and pre-flood forest composition;
3. **Damaged tree volume and volume per hectare also tended to increase with increasing drainage area.** Drainage area accounted for more variance in damaged tree volume per hectare ($R^2 = 0.81$, p-value =0.01) and for valley bottom landforms ($R^2 = 0.02 – 0.92$);
4. **Geomorphic stream power is a good predictor of tree damage.** Cross-sectional and mean 500-year stream power estimates explained for the most variance in canopy loss ($R^2 = 0.73$ and $R^2 = 0.70$) and damaged tree volume ($R^2 = 0.90$ and $R^2 = 0.67$). Additionally, mean stream power showed relatively high correlations with other geomorphic variables and represents the combined effects of slope, sinuosity, and confinement;
5. **Floodplains and terraces tended to have the greatest quantities of tree damage.** Four of the six sites had the greatest damaged tree volume occur on floodplains and terraces. When present, chutes typically had the least damaged tree volume. However, chutes can direct flows into forested areas on higher elevations, potentially causing tree damage; and
6. **The use of UAVs proved to be a useful tool for detecting and measuring riparian forest damage.** Field and UAV volume estimates showed high R^2 (0.91) and were statistically significant (p-value < 0.01). Errors were generally understood, however more work on these applications is needed.

This work provides much needed data on the relationship between large flood effects and riparian forest damage in the Ozark Highlands. This region lacks this kind of data and has increasing concerns of larger more frequent floods (Pavlowsky et al., 2016; Heimann et al.,

2018). Future work will focus on collecting data at more sites to increase the sample size and verify the relationships between the hydrologic/geomorphic variables and forest damage and creating accurate predictive models of riparian forest damage. Mean and cross-sectional stream power accounted for the most variance in total damaged tree volume and canopy loss and could be used as predictors of forest damage. However, with only a small sample size (n = 6) more sample sites are needed to verify these relationships. UAVs were also verified as accurate time-saving tools for assessing forest damage. These results further our understanding of flood effects on riparian forests and contributes to our broader understanding of the effects of climate change. With increasing concerns about climate change, the demand for more studies on its effects on watersheds are needed.

Table 1. Alluvial Soil Series at the Sample Reaches

	Relfe-Sandbur Complex	Secesh-Tilk Complex	Britwater Silt-Loam
Soil Order	(Ap/C)	(Ap/BE/Bt/2Bt)	(Ap/Bt1/2Bt2)
Flood Frequency	Frequent	Occasional	Rare
Landform	Floodplains	Floodplains	Terraces
Texture			
Surface Soil	Very gravelly sandy loam	Silt loam	Silt loam
Subsoil	Extremely cobbly coarse sand and very gravelly loamy sand	Gravelly clay loam	Very gravelly clay loam
Thickness			
Surface Soil	15 cm	70 cm	60 cm
Subsoil	> 135 cm	> 80 cm	> 90 cm
Depth to Bedrock	> 150 cm	> 150 cm	> 150 cm
Sample Reach Area (%)			
Dry Creek	73	0	37
Indian Creek	100	0	0
Lower Tabor Creek	100	0	0
Upper Tabor Creek	0	100	0
Spring Branch	100	0	0
Lick Branch	0	100	0

Table 2. Watershed Characteristics

Site	Drainage Area (km^2)	% Area MTNF	Basin Slope (m)	2016 Land Use (%)			
				Agriculture	Forest	Urban	Other
Dry Creek	124.2	36	0.006	31	64	4	1
Indian Creek	101.6	43	0.007	16	79	3	2
Lower Tabor Creek	65.4	19	0.013	43	51	6	0
Upper Tabor Creek	54.0	7	0.005	50	45	3	2
Spring Branch	49.1	50	0.008	19	78	2	1
Lick Branch	4.5	62	0.013	13	86	1	0

Table 3. Geomorphic Site Characteristics

	Dry Creek	Indian Creek	Lower Tabor Creek	Upper Tabor Creek	Spring Branch	Lick Branch
Sinuosity	1.1	1.2	1.8	1.0	1.3	1.2
Active Channel Width (m)						
Average	19.9	31.5	47.9	28.6	25.8	13.3
CV%	34	25	32	10	48	21
Valley Width (m)						
Average	103.3	100.5	56.7	65.5	127.5	58.7
CV%	16	10	45	27	14	5
Confinement Ratio						
Average	5.8	3.3	1.2	2.3	5.8	4.6
CV%	43	24	35	33	40	20
Channel bed Material						
Sample size	29	30	30	30	30	15
D16	13.6	19.9	14.8	8	5	32
D50	35	39.5	48.5	16	27.5	64
D84	60.4	74.2	90.2	45	60.2	118
Average Max Clast Size (mm)	512	165.8	286	196	108	182
% Bedrock/Cut-Earth	3	0	0	0	0	50
Reach Slope (m/m)	0.007	0.003	0.011	0.005	0.004	0.015

Table 4. Landform Distribution

	Dry Creek	Indian Creek	Lower Tabor Creek	Upper Tabor Creek	Spring Branch	Lick Branch
Study Area (ha)	2.08	4.01	4.80	2.04	3.47	0.26
% Active Channel	28	10	30	49	18	36
% Floodplain	39	17	34	39	34	64
% Terrace	22	67	24	12	46	0
% Chute	11	6	12	0	2	0

Table 5. 500-year Flood

	Dry Creek	Indian Creek	Lower Tabor Creek	Upper Tabor Creek	Spring Branch	Lick Branch
Width (m)	117.25	123.80	96.78	80.70	131.35	26.12
Depth (m)	5.10	5.60	4.00	3.80	3.70	2.10
Hydraulic Radius (m)	2.78	3.19	1.91	2.01	2.00	0.30
Velocity (m/s)	2.12	1.60	3.26	2.10	1.51	2.02
Area (m^2)	332.31	410.26	187.94	164.90	268.12	8.21
Wetted Perimeter (m)	119.72	128.79	98.15	82.05	134.28	26.93
Width -Depth Ratio	22.99	22.11	24.20	21.24	35.50	12.44
Discharge (m^3/s)	735.12	674.80	634.47	343.16	410.26	75.61
Mean 500-year SP (W/m^2)	347	492	847	207	249	349
Cross-Sectional 500-year SP (W/m)	43,377	46,299	77,877	16,858	33,466	9,748
HWM Flood Depth (m)	7.30	5.60	7.70	6.70	4.60	3.20
Difference in 500year and HWM Flood Stage (m)	2.20	0.00	3.70	2.90	0.90	1.10
HWM Height Range (m)	1.18	2.35	3.28	6.01	2.87	1.54

Table 6. Pre and Post Flood Canopy Cover

	Dry Creek	Indian Creek	Lower Tabor Creek	Upper Tabor Creek	Spring Branch	Lick Branch
Pre-Flood Open Canopy (%)						
Total	5	19	1	0	12	0
Active Channel	5	16	0	0	10	0
Floodplains	0	3	0	0	2	0
Terraces	0	0	0	0	0	0
Chutes	0	0	0	0	0	0
Canopy Loss (%)						
Total	31	32	63	28	8	7
Active Channel	24	42	38	94	48	56
Floodplain	17	28	44	3	52	44
Terrace	55	30	3	4	0	0
Chute	5	0	16	0	0	0

Table 7. Riparian Forest Damage at each Site

	Dry Creek	Indian Creek	Lower Tabor Creek	Upper Tabor Creek	Spring Branch	Lick Branch
Standing Trees						
Count	269	212	273	187	266	75
% in Active Channel	18	6	14	36	6	31
% on Floodplains	63	9	23	51	36	69
% on Terraces	13	83	56	13	59	N/A
% in Chutes	6	2	7	N/A	0	N/A
Damaged Trees						
Count	193	170	393	206	56	14
% in Active Channel	10	13	23	50	20	64
% on Floodplains	26	21	50	27	57	36
% on Terraces	48	59	16	23	20	0
% in Chutes	15	7	11	0	4	0
Average Damaged Tree Diameter (m)						
Active Channel	0.22	0.22	0.20	0.17	0.29	0.15
Floodplains	0.18	0.23	0.16	0.13	0.25	0.15
Terraces	0.18	0.21	0.18	0.16	0.26	N/A
Chutes	0.18	0.22	0.17	N/A	0.18	N/A

Table 7 continued. Riparian Forest Damage at each Site

	Dry Creek	Indian Creek	Lower Tabor Creek	Upper Tabor Creek	Spring Branch	Lick Branch
Average Damaged Tree Length (m)						
Active Channel	8.6	12.4	8.4	8.8	11.7	4.4
Floodplain	8.7	10.2	9.0	6.3	9.5	6.5
Terraces	8.0	8.1	8.5	6.3	10.3	N/A
Chutes	7.1	8.5	8.3	N/A	10.5	N/A
Damaged Tree Volume (m^3)						
Total	56.8	84.7	114.1	36.4	35.2	1.4
Active Channel	8.9	13.1	35.1	24.7	10.7	0.7
Floodplain	14.5	24.7	49.3	5.3	17.8	0.7
Terraces	24.6	41.9	19.7	6.4	6.1	N/A
Chutes	8.7	5.0	10.0	N/A	0.5	N/A
Damaged Tree Volume (m^3) / hectare						
Total	30.7	28.3	27.1	17.9	10.4	5.2
Active Channel	17.1	42.0	28.1	24.5	17.7	7.3
Floodplains	20.1	49.5	34.2	6.7	15.5	4.0
Terraces	60.1	21.0	19.2	26.3	3.9	N/A
Chutes	43.3	27.2	20.2	N/A	9.3	N/A

Table 8. Standing Basal Area and Stored Wood Volume within the 5 m wide Sampling Zone

Site	Transect	Standing Basal Area (m^2/ha)	Wood Volume (m^3)
Dry Creek	4	17.4	1.32
Indian Creek	4	17.6	2.86
Indian Creek	7	15.4	3.54
Lower Tabor Creek	3	9.9	2.55
Upper Tabor Creek	3	19.9	2.1
Spring Branch	5	4.4	4.89
Spring Branch	7	29.5	0.58
Lick Branch	1	68.5	0
Lick Branch	4	48.2	0.71
Lick Branch	10	2.5	0

Table 9. Correlation Matrix of Geomorphic Variables and Forest Damage

	Mean 500-year SP	Cross-Sectional 500-year SP	Drainage Area	Basin Slope	Reach Slope	Sinuosity	Confinement	D50	Avg. Max Clast
Damaged Tree Volume (m^3)									
Total	**0.82	***0.95	0.60	0.01	-0.24	0.65	-0.56	-0.03	0.26
Active Channel	0.52	0.55	0.14	-0.10	-0.22	0.48	***-0.89	-0.37	-0.09
Floodplain	***0.93	***0.91	0.44	0.24	-0.02	*0.71	-0.63	0.23	0.18
Terrace	0.33	*0.70	**0.80	-0.25	-0.50	0.28	0.27	-0.15	0.38
Chute	0.61	**0.79	***0.83	-0.09	-0.10	0.36	-0.07	0.11	*0.74
Damaged Tree Volume per Hectare (m^3/ha)									
Total	0.43	*0.69	***0.90	-0.43	-0.35	0.18	-0.26	-0.29	*0.72
Active Channel	0.28	0.43	0.13	-0.28	-0.41	0.38	*-0.70	-0.61	-0.16
Floodplain	0.59	*0.72	***0.84	-0.14	-0.19	0.23	-0.14	0.14	0.59
Terrace	-0.02	0.36	***0.87	*-0.71	-0.49	-0.14	0.06	-0.58	*0.76
Chute	0.40	0.63	***0.91	-0.26	-0.24	0.11	0.11	0.04	*0.74

*Significant at the 90% confidence level **Significant at the 95% confidence level ***Significant at the 98% confidence level

Table 9 continued. Correlation Matrix of Geomorphic Variables and Forest Damage

	Mean 500-year SP	Cross-Sectional 500-year SP	Drainage Area	Basin Slope	Reach Slope	Sinuosity	Confinement	D50	Avg. Max Clast
Canopy Loss (%)									
Total	***0.84	***0.86	0.45	0.09	0.03	0.66	*-0.74	0.02	0.41
Active Channel	-0.46	*-0.75	*-0.72	0.02	0.20	-0.42	-0.27	-0.09	-0.55
Floodplain	***0.87	**0.79	0.40	0.33	0.05	0.58	-0.45	0.44	0.12
Terrace	-0.33	0.08	0.47	-0.36	-0.31	-0.13	**0.79	-0.30	0.50
Chute	***0.83	***0.97	0.46	0.27	0.08	***0.83	-0.30	0.16	0.47

*Significant at the 90% confidence level **Significant at the 95% confidence level ***Significant at the 98% confidence level

Table 10. Correlation Matrix of Geomorphic and Hydrologic Variables

	Mean 500-year SP	Cross-Sectional 500-year SP	Drainage Area	Basin slope	Reach Slope	Sinuosity	Confinement	D50	Avg. Max Clast
Mean 500-year SP	1.00								
Cross-Sectional 500-year SP	***0.86	1.00							
Drainage Area	0.16	0.52	1.00						
Basin Slope	0.56	0.19	-0.61	1.00					
Reach Slope	0.33	-0.08	-0.58	***0.84	1.00				
Sinuosity	***0.86	**0.80	-0.08	0.65	0.33	1.00			
Confinement	-0.62	-0.42	0.10	-0.20	-0.13	-0.47	1.00		
D50	0.49	0.10	-0.37	***0.87	**0.82	0.35	-0.02	1.00	
Avg. Max Clast	0.18	0.33	0.64	-0.19	0.15	0.01	0.16	0.03	1.00

*Significant at the 90% confidence level **Significant at the 95% confidence level ***Significant at the 98% confidence level

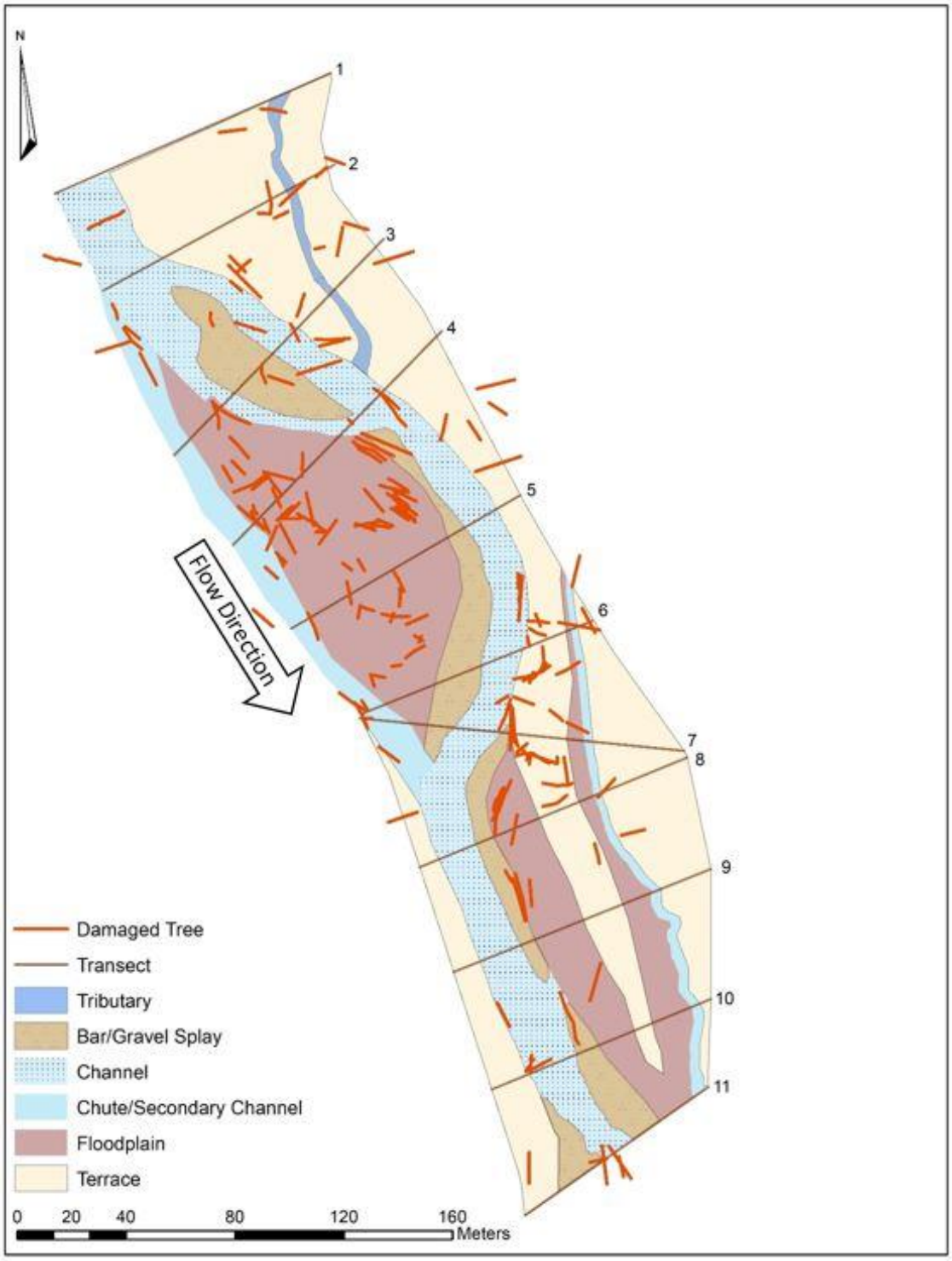

Fig. 3a. Geomorphic Map of Indian Creek

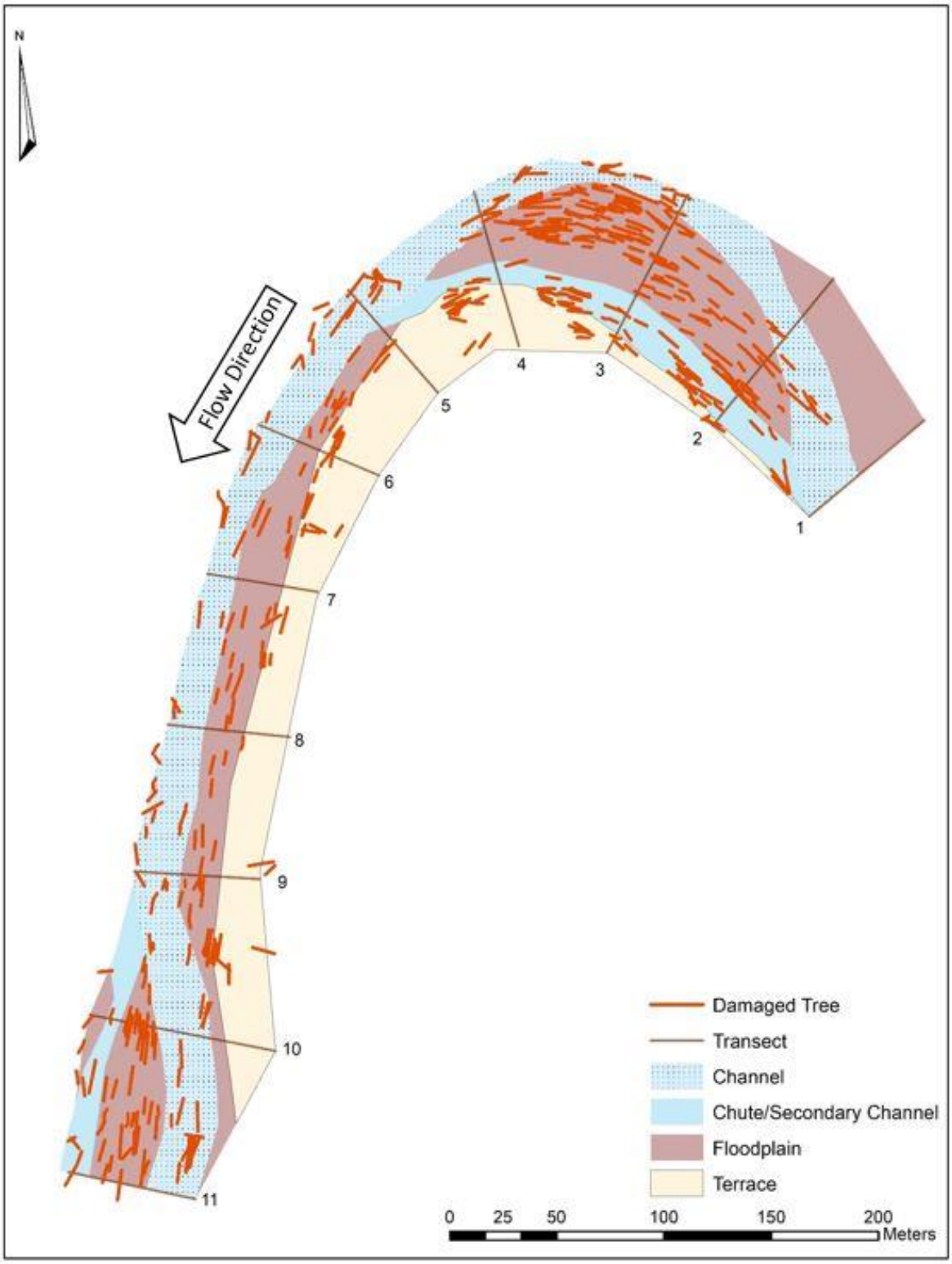

Fig. 3b. Geomorphic Map of Lower Tabor Creek

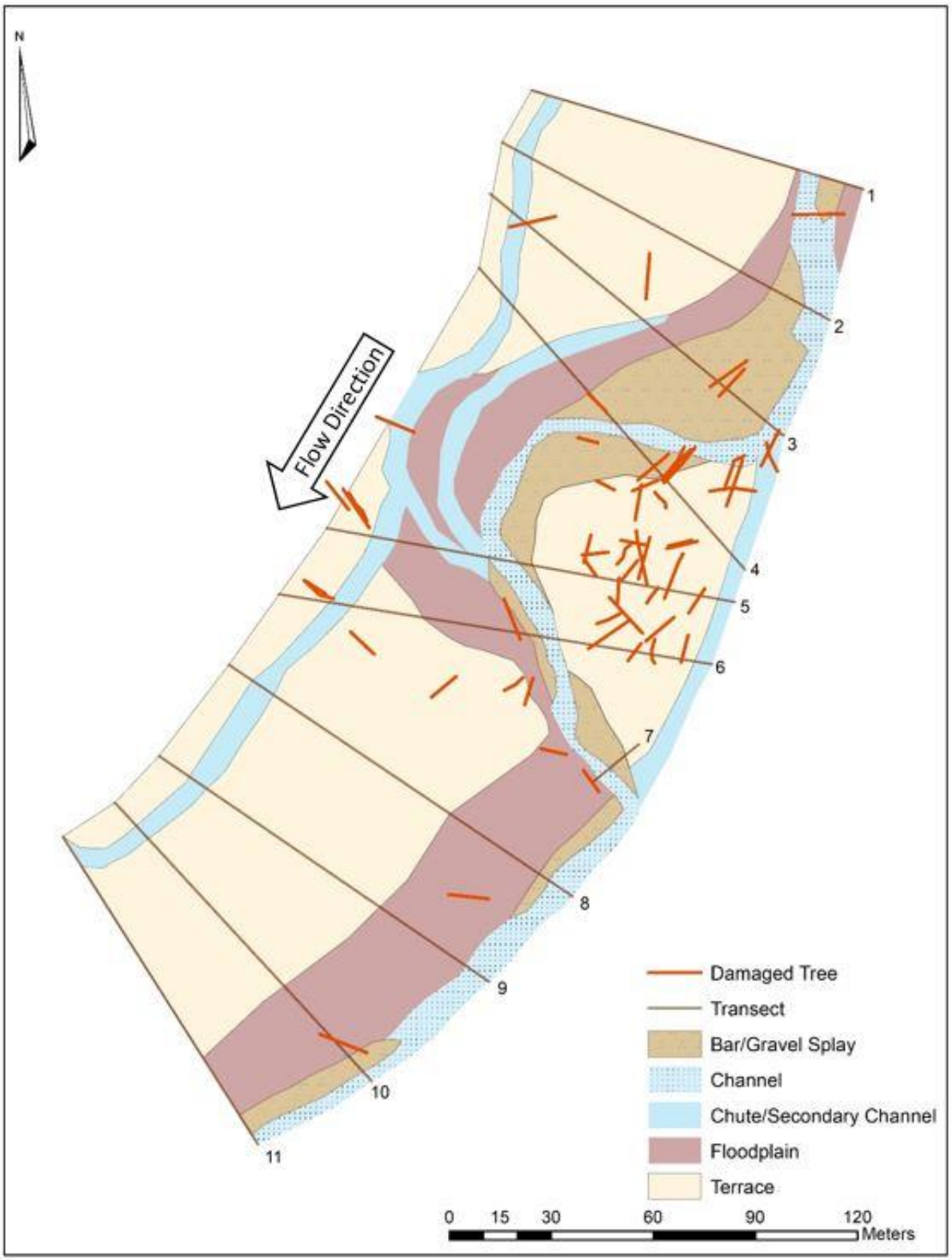

Fig. 3c. Geomorphic Map of Spring Branch

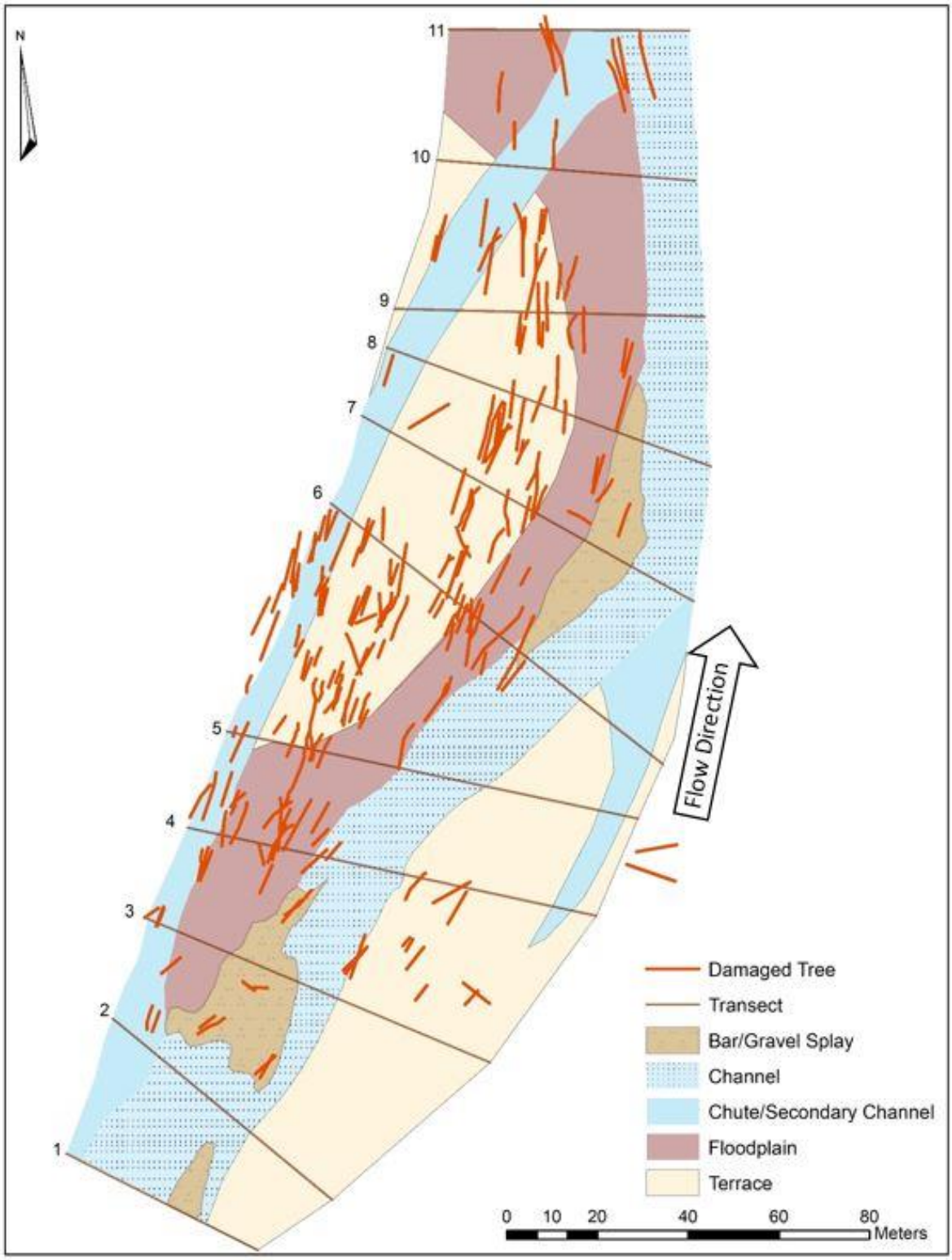

Fig. 3d. Geomorphic Map of Dry Creek

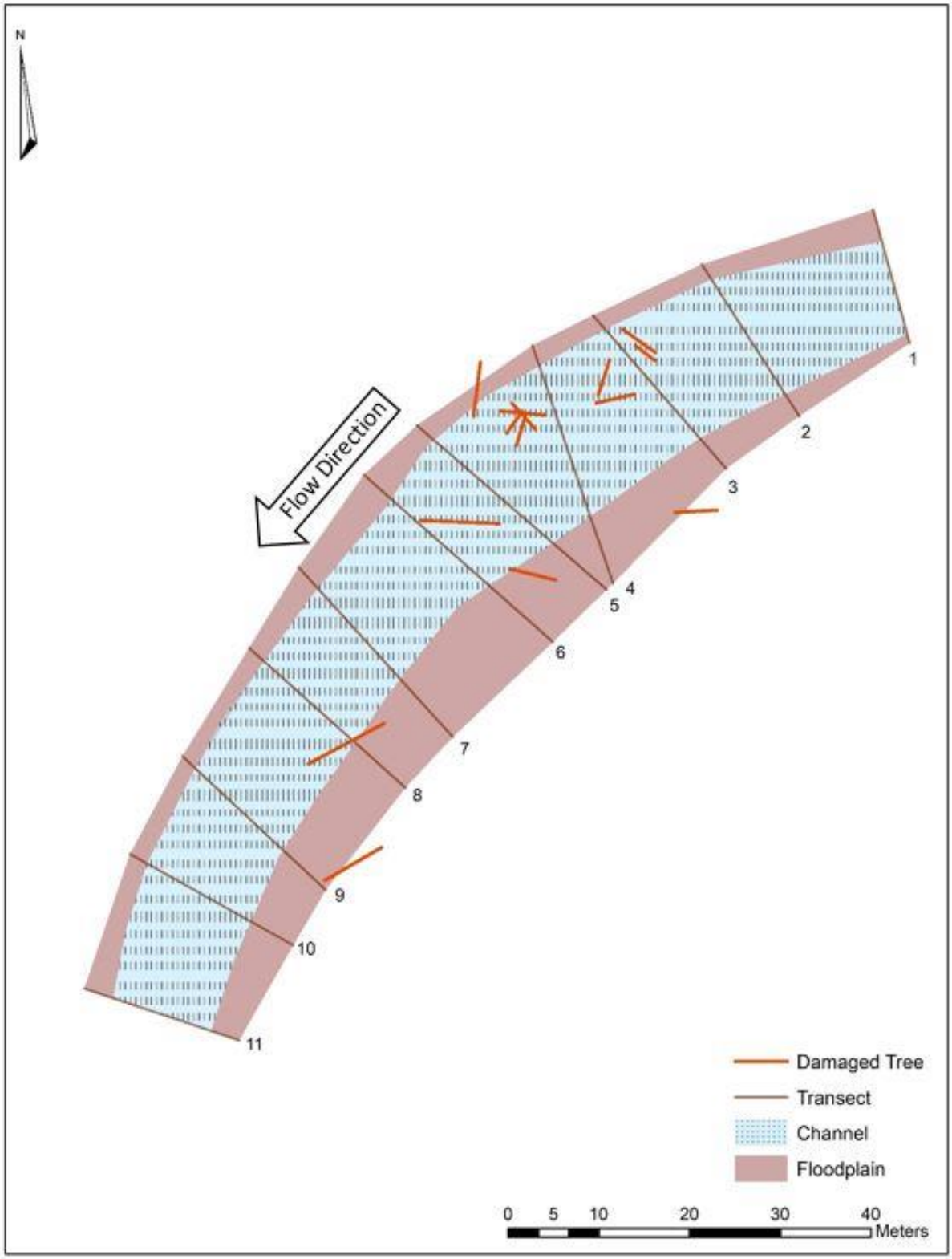

Fig. 3e. Geomorphic Map of Lick Branch

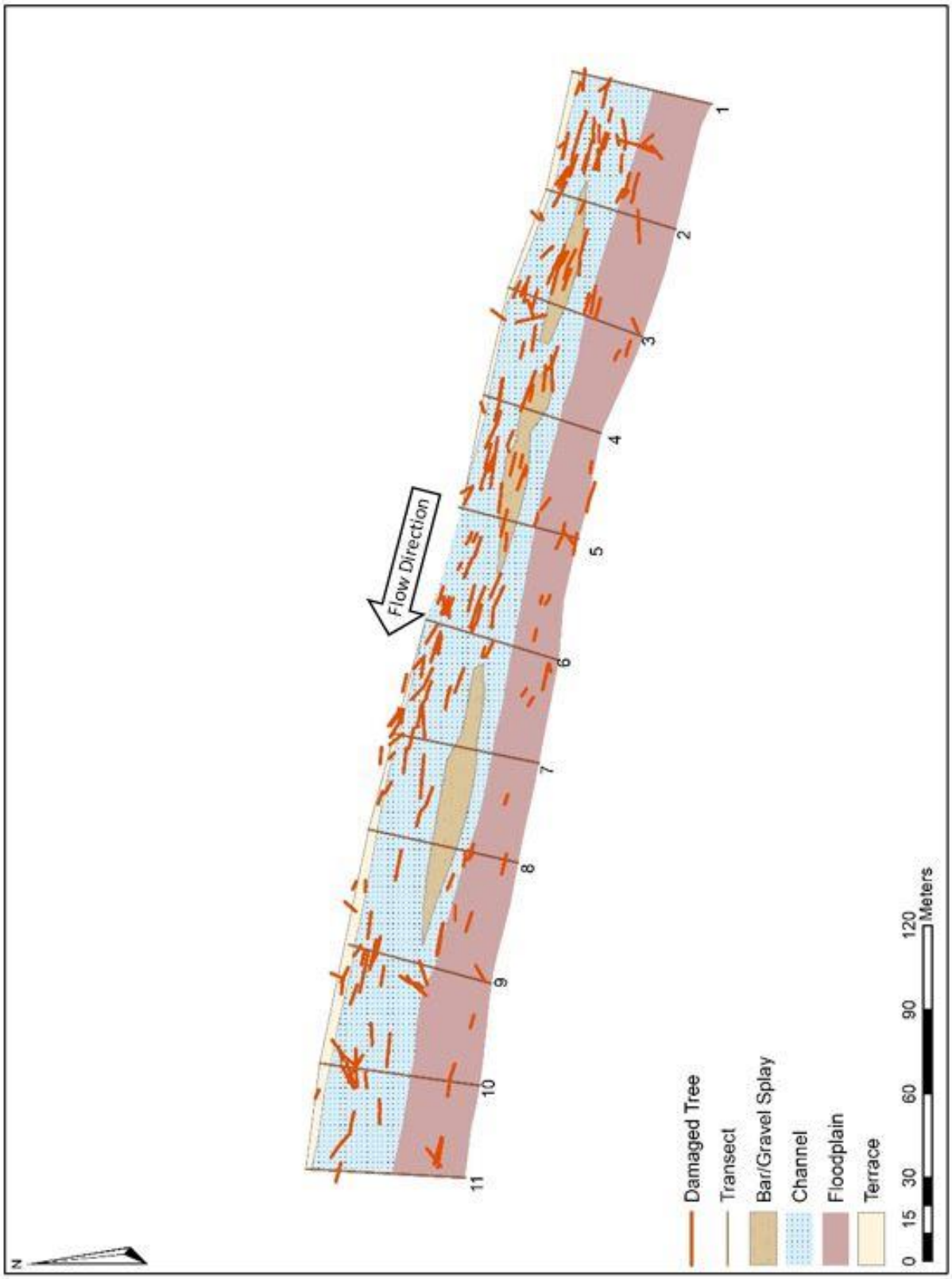

Fig. 3f. Geomorphic Map of Upper Tabor Creek

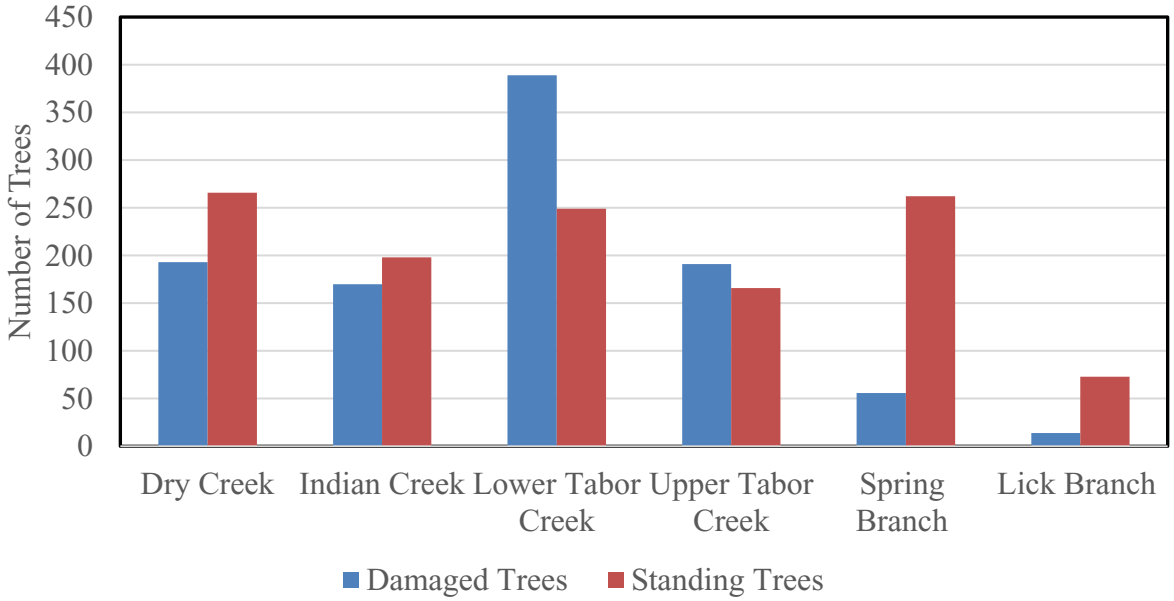

Fig. 4. Number of Standing and Down Trees

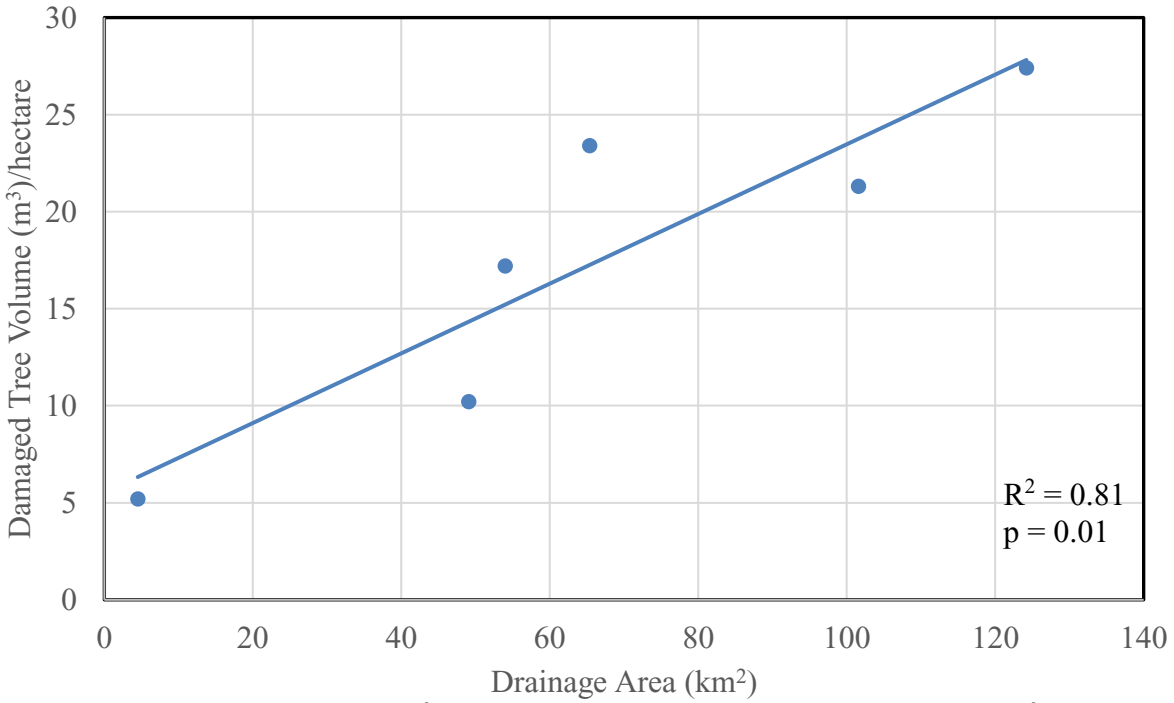

Fig. 5. Damaged Tree Volume (m^3) per Hectare Compared to Drainage Area (km^2)

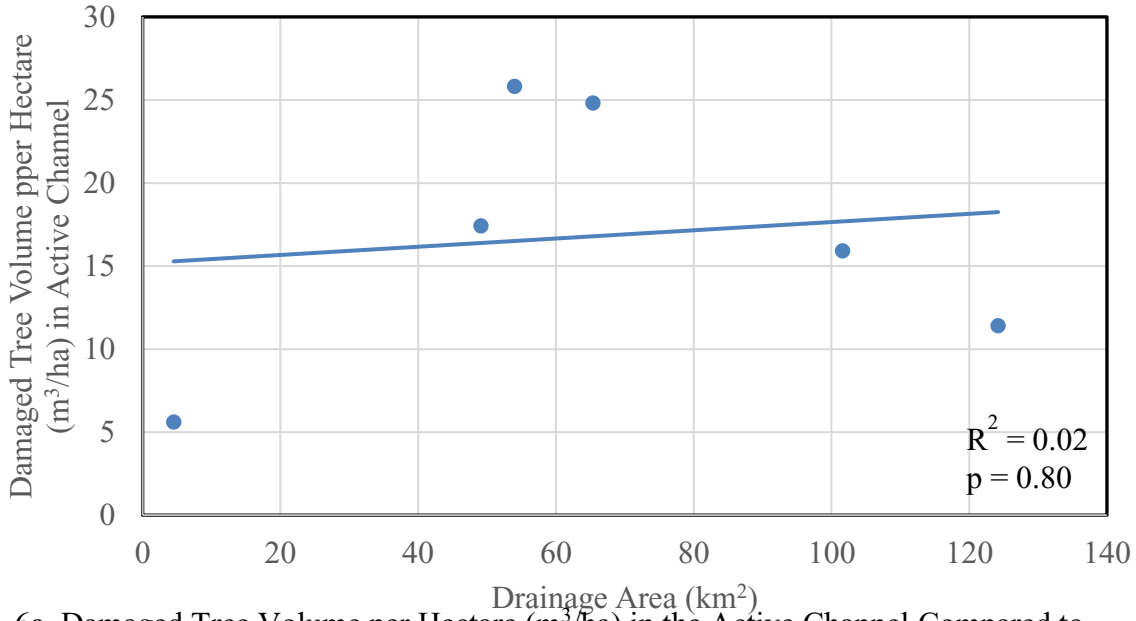

Fig. 6a. Damaged Tree Volume per Hectare (m^3/ha) in the Active Channel Compared to Drainage Area (km^2)

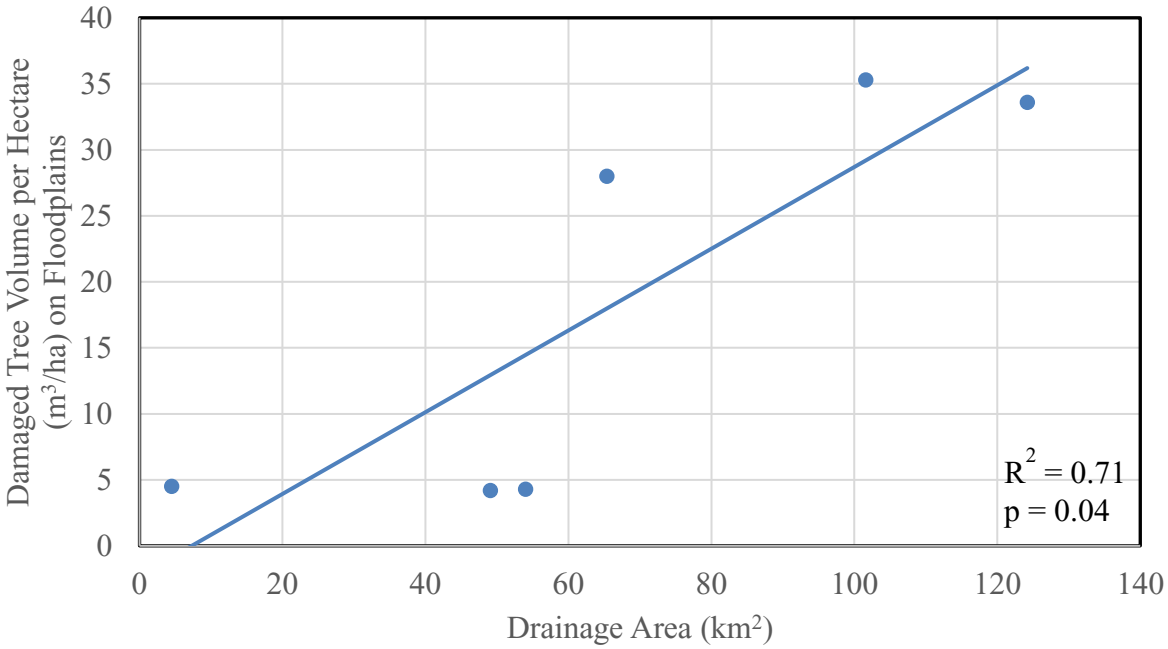

Fig. 6b. Damaged Tree Volume per Hectare (m^3/ha) on Floodplains Compared to Drainage Area (km^2)

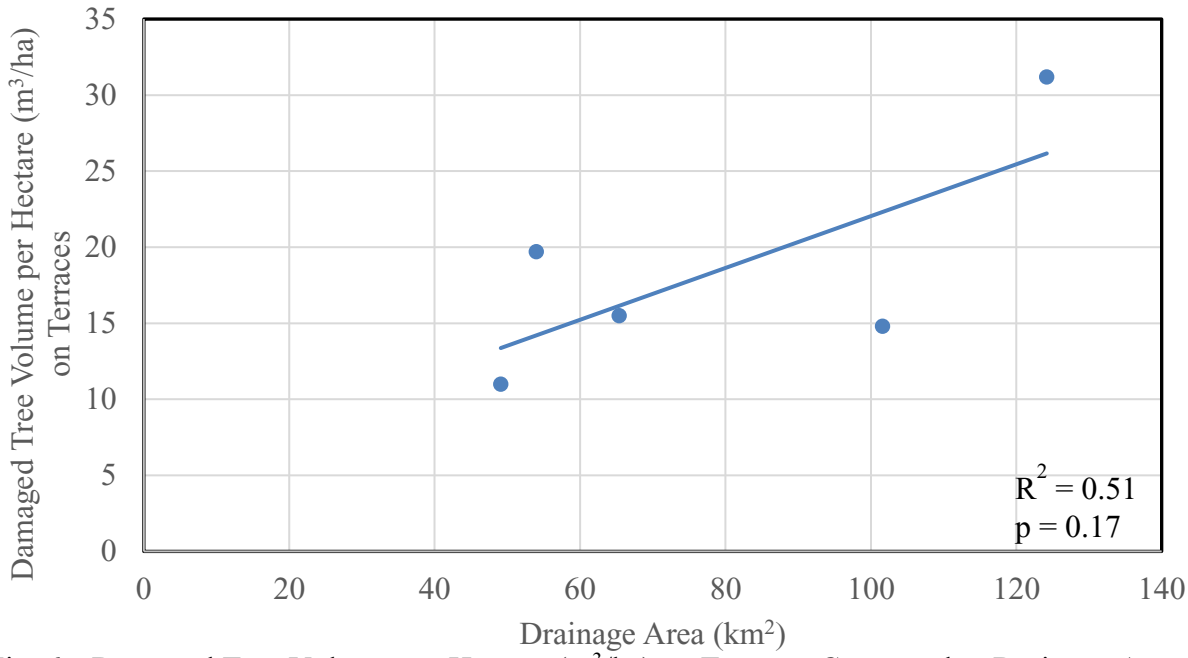

Fig. 6c. Damaged Tree Volume per Hectare (m^3/ha) on Terraces Compared to Drainage Area (km^2)

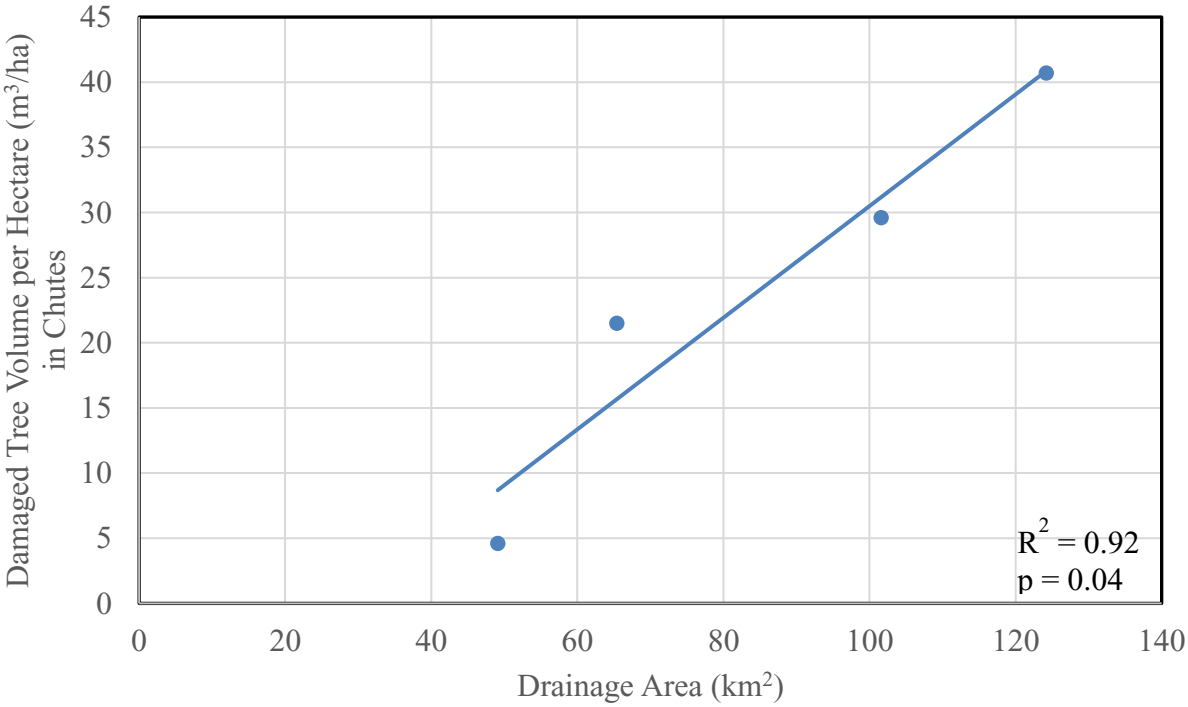

Fig. 6d. Damaged Tree Volume per Hectare (m^3/ha) in Chutes Compared to Drainage Area (km^2)

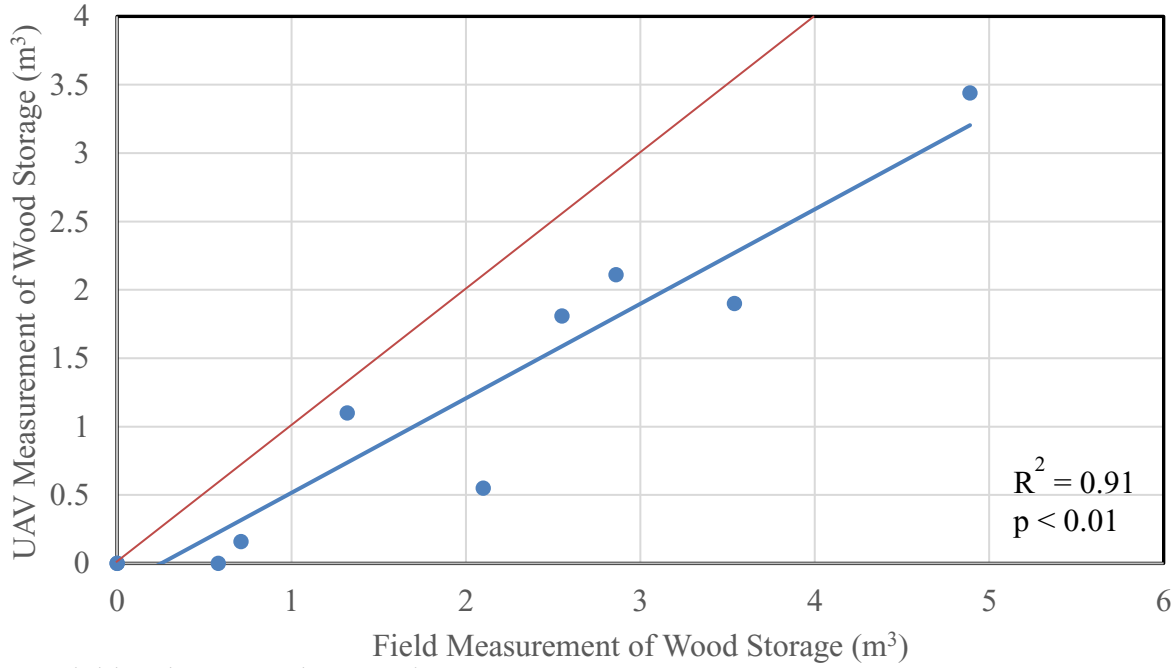

Fig. 7. Field and UAV Volume Estimates

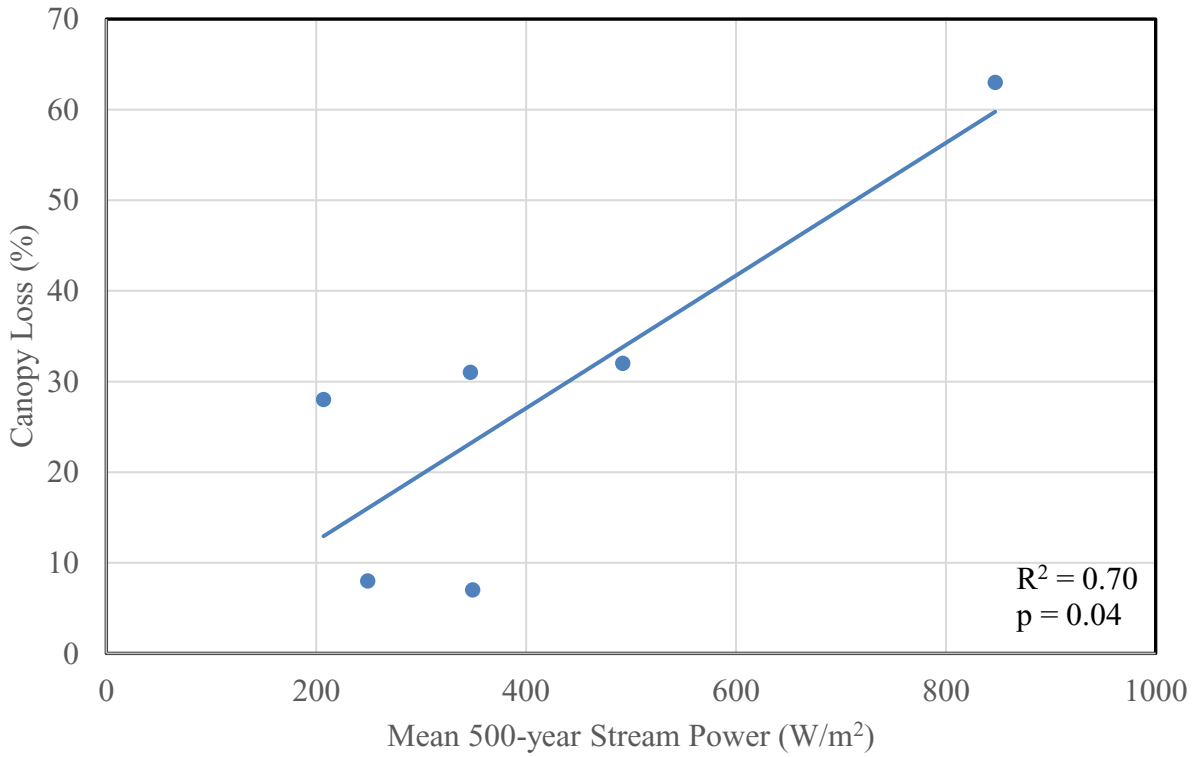

Fig. 8a. Mean 500-year Stream Power (W/m^2) Compared to Canopy Loss (%)

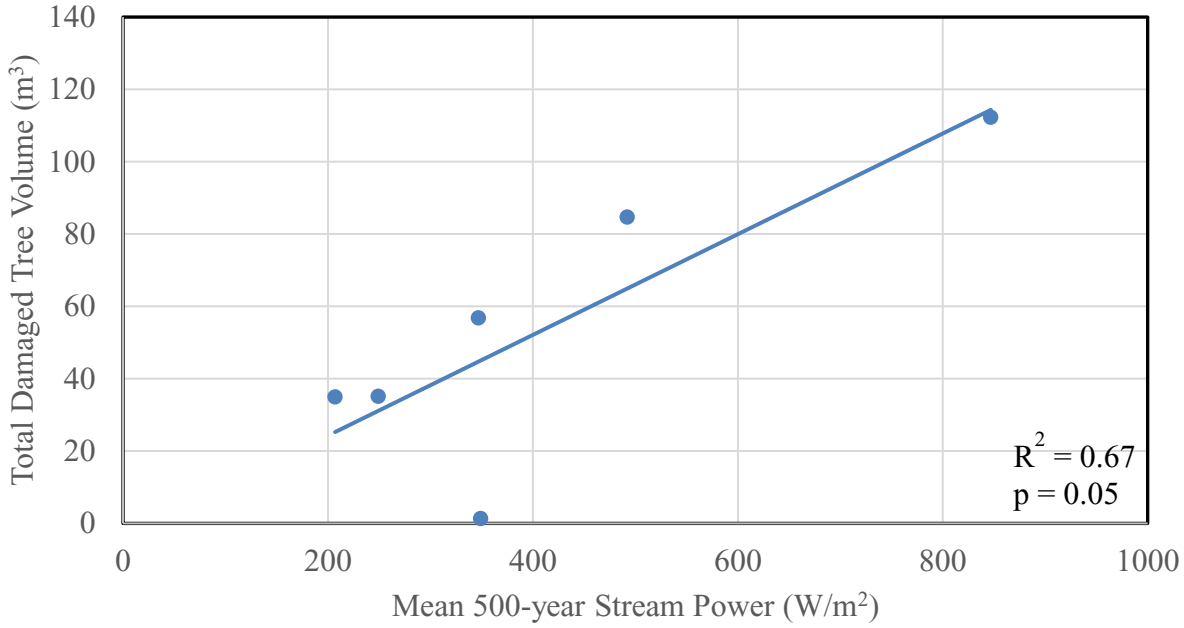

Fig. 8b. Mean 500-year Stream Power (W/m^2) Compared to Total Damaged Tree Volume (m^3)

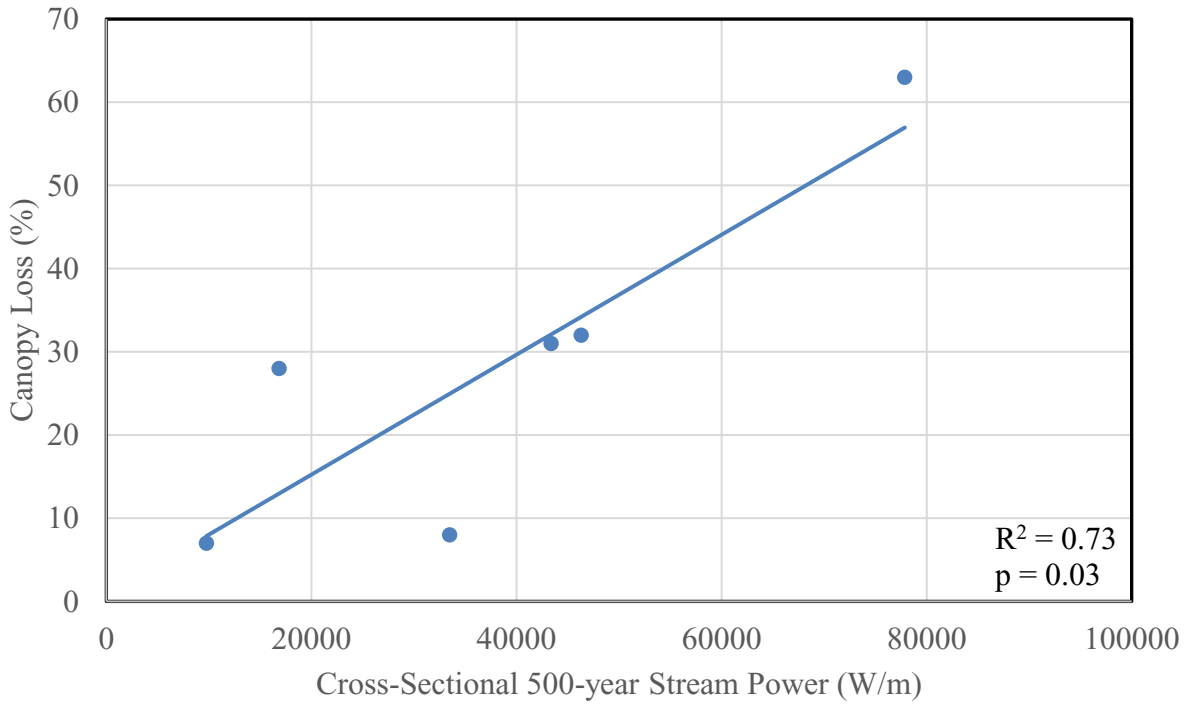

Fig. 9a. Cross-Sectional 500-year Stream Power (W/m) Compared to Canopy Loss (%)

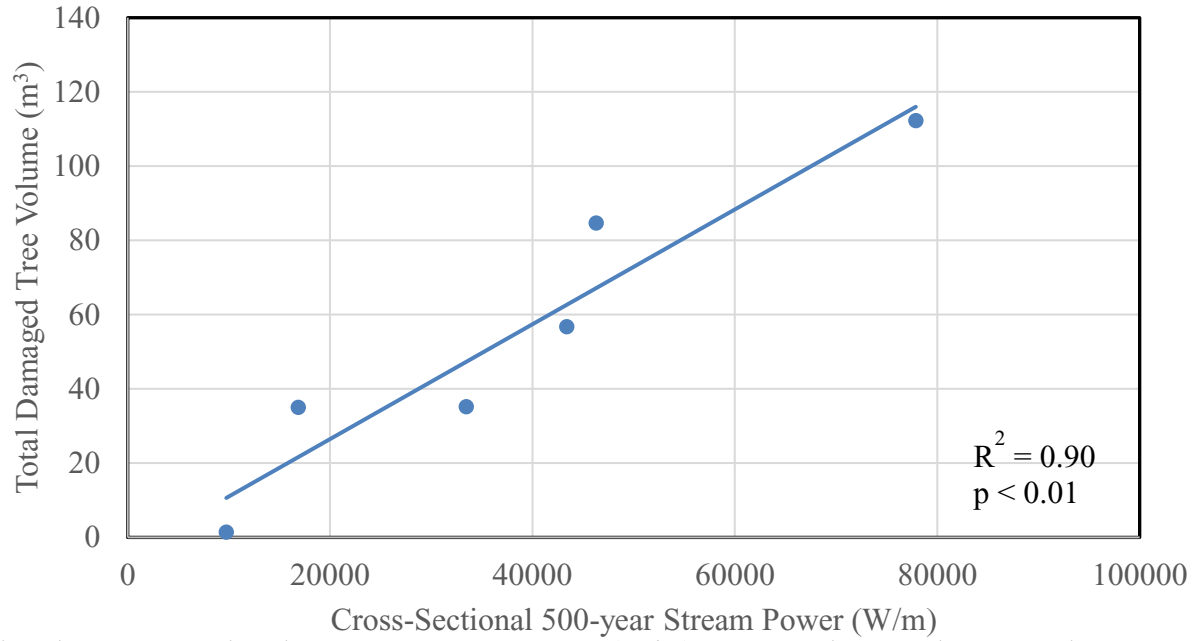

Fig. 9b. Cross-Sectional 500-year Stream Power (W/m) Compared to Total Damaged Tree Volume (m^3)

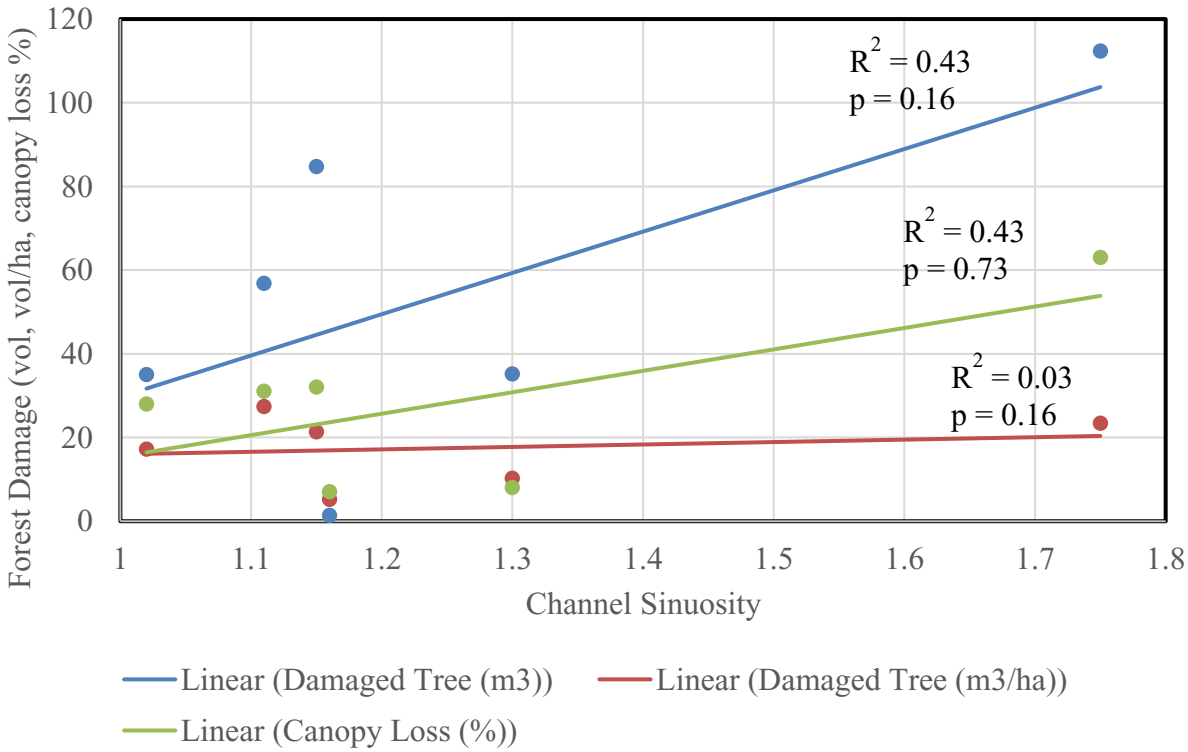

Fig. 10. Forest Damage Compared to Channel Sinuosity

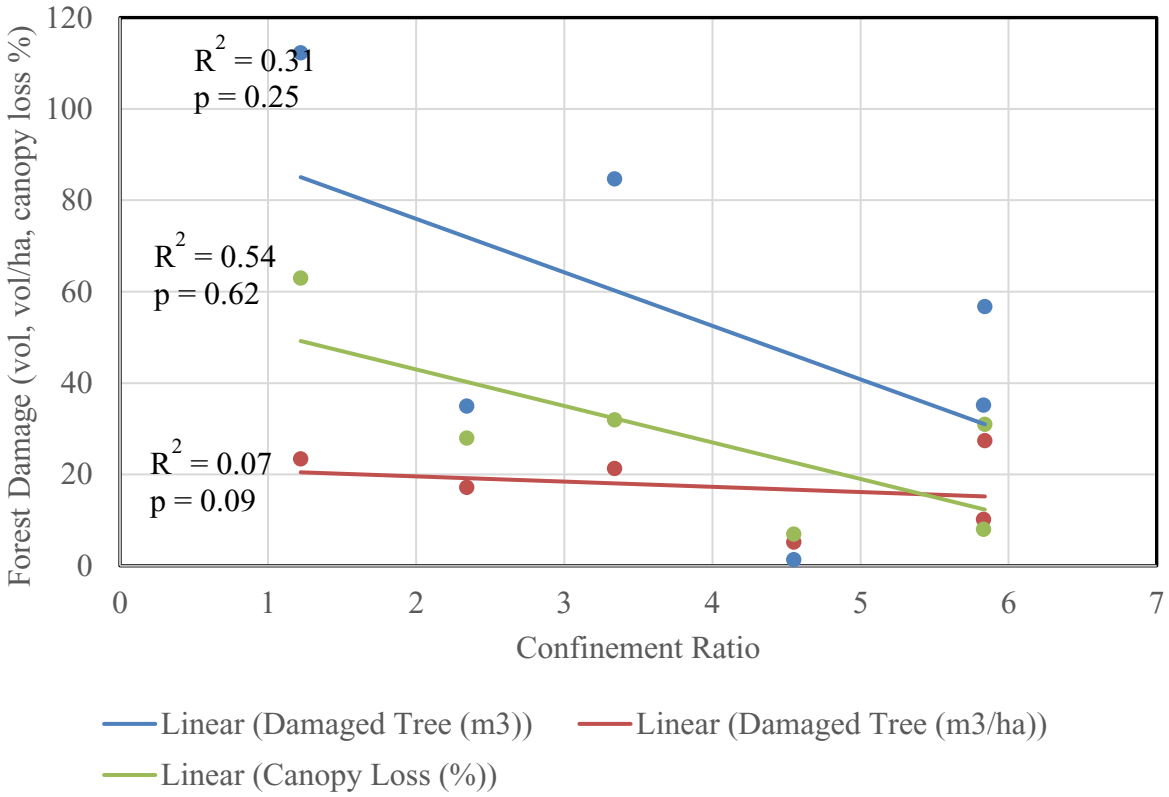

Fig. 11. Forest Damage Compared to Valley Confinement

CHAPTER THREE: UAV MONITORING OF FOREST DAMAGE AND FLUVIAL LANDFORMS

Unmanned aerial vehicles (UAVs) have previously been used to acquire high-resolution aerial imagery to provide detailed information for environmental assessments (Quilter and Anderson, 2000; Dandois and Ellis, 2010; Anderson and Gaston, 2013; Jeong et al., 2018). The need for UAV imagery in this study comes after a 500-year flood event in the Missouri Ozarks, which caused extensive damage to riparian forests. The purpose of this chapter is to assess whether the use of UAV imagery can accurately assess riparian forest damage along six sites following the 500-year flood event. UAV imagery has the potential to quickly quantify and identify patterns of riparian forest damage that would normally take weeks to accomplish with field surveys. The objectives of this study are to assess the accuracy of UAV imagery in detecting individual damaged tree volume, canopy change, and stream geomorphology. If successful, UAVs could help support forest management practices in Mark Twain National Forest and further support the use of UAVs in environmental assessments.

The high-resolution imagery that UAVs can obtain has allowed for precise assessments of forest and river characteristics. UAV imagery has been used before to identify individual plants and canopy gaps greater than one square meter (Getzin et al., 2012). Additionally, with the use of photogrammetry, UAV images can produce three-dimensional models to derive heights of landforms (Dandois and Ellis, 2010; Watanabe and Kawahari, 2016) and canopy heights (Zahawi et al., 2015). The accuracy of three-dimensional models produced from UAV imagery has been tested with promising results. In a comparison of a digital surface model (DSM) derived from UAV imagery with a ground survey of river channel morphology, Watanabe and Kawahari

(2016) found similar results, with an average difference in elevation of only 4 cm and a maximum difference of 7 cm. Photogrammetric techniques were limited by thick vegetation, which prevented accurate ground level data to be acquired with the UAV (Watanabe and Kawahari, 2016).

Image collection procedures affect the accuracy of measurements derived from aerial photographs and photogrammetric techniques. In a study on the accuracy of UAV photogrammetric mapping of a beach environment, Jeong et al. (2018) obtained root mean square errors (RMSEs) of less than 4.9 cm with flight altitudes less than 150 m and image overlap of 70%. Similarly, Dandois et al., (2015) found that clear skies, image overlap of greater than 60% and 80 m flight altitude (above forest canopy) provides optimal UAV-SfM (structure-from-motion) remote sensing conditions. Ground control points (GCPs) are also crucial for obtaining accurate images. Jeong et al., (2018) had RMSEs of less than 9.4 cm when using at least five GCPs. The accuracy of aerial photographs can be verified through field surveys (Fujita et al., 2003) or through other forms of imagery such as LiDAR (Dandois et al., 2015; Jeong et al., 2018). For this study ground surveys were conducted to check UAV measurements.

Modern photogrammetry uses Structure-from-Motion (SfM) techniques which allow measurements to be derived from aerial photographs (Fonstad et al., 2013). SfM photo-grammetry uses photos taken from several perspectives to create three-dimensional shapes of objects in the photographs (Fonstad et al., 2013). SfM photogrammetry works by identifying key points in the photographs (key points are unique points in the photographs) and then using the key points to find tie points (the same point identified in different photographs) (Warrick et al., 2017). Once the tie points are identified, the camera position can be identified in the model and this allows for three dimensional point clouds and models to be built (Warrick et al., 2017).

Study Area

This study was conducted in southern Missouri on tributaries of the North Fork of the White River in the counties of Douglas and Howell (Fig. 1). Six sites, along different tributary streams, were selected to identify how well UAV imagery can detect forest damage (i.e., individual tree volume and canopy change) and fluvial landforms along streams that suffered catastrophic damage due to the large flood (>500-year RI) (Erdman, 2017; US Department of Commerce, 2017 Heimann et al., 2018). The sites cover a range of drainage areas (4.5 – 124.2 km^2) with access to Mark Twain National Forests and where the most precipitation fell during the storm event which led to the flooding (Fig. 1, Fig. 2).

Methods

Imagery Collection. High-resolution (< 8 cm) UAV imagery was collected at six tributary sites with a DJI Phantom 4 Pro in March 2018. The DJI Phantom 4 Pro has a 1" CMOS sensor and a maximum flight time of approximately 30 minutes (DJI Phantom 4 Pro, 2019). Agisoft Metashape (formerly Agisoft Photoscan Professional) was used to process the UAV imagery and generate high-resolution orthophotos and Digital Surface Models (DSMs) (Agisoft Metashape, 2019). Gradual selection processes were used to filter points that had high residual errors (Hostens, 2019).

The UAV imagery was collected during the early spring months in 2018 to allow more ground-level forest damage to be better detected due to the lack of leaf cover (Benke et al., 2000). The September 2017 imagery, showed the sites with leaves on the trees and these images were used to calculate changes in canopy cover. Ground control points (GCPs) were used to improve the accuracy of the UAV images (Vanlooy and Martin, 2005). Typically, six GCPs were

used at each site, however, the number of GCPs varied at the largest and smallest site. Lick Branch only used five GCPs, while Lower Tabor Creek used ten. The UAV flight altitude was 108 m and front and side image overlap was 80%. Several flight plans were used to acquire the images, including North-South Orthogonal, North-South Oblique, East-West Orthogonal, and East-West Oblique. The final images were generated from a combination of all the flight plans.

Field Methods. Cross-sections of the valley floor, including the channel, floodplains, terraces, and chutes, were surveyed in the field (September 2018) to compare with cross-sections from the UAV DSM (March 2018). Measuring tapes were placed perpendicular to the stream and pulled across the valley floor. Elevation data was then collected along the tape using a stadia rod and an auto-level. In April, 2019 riparian tree sampling was conducted in the field at transects within a 5 m wide grid using the transect line as the upstream limit of the zone. Transect sampling is the recommended sampling method for areas influenced by an environmental gradient (Lyons and Sagers, 1998). Riparian tree sampling was performed in order to test the accuracy of the UAV measurements. One to three transects perpendicular to the streams were collected at each site and used as a baseline for a 5 m wide sample belt of riparian forest, similar to a study done by Katz et al. (2005). Tree diameter and length were recorded for all toppled or uprooted trees. Tree diameter was measured in two ways, once within the 5 m wide transect zone and once for the whole tree. Both field measurements of tree diameter were compared to the UAV measurement. Only whole tree length was compared to the UAV measurements. In the literature, there is large variation in the minimum tree diameter recorded in forest sampling procedures, ranging from 2-20 cm (Everham and Brokaw, 1996). For this study, 10 cm was the minimum tree diameter that was included (Fierke and Kauffman, 2006). Standing tree and uprooted/toppled tree locations (x-y coordinates) were recorded to compare with UAV

imagery and assess the accuracy of GIS methods (Allen et al., 2012). Additionally, tree azimuth and some species identification data were collected.

GIS Methods. (See previous methods reported in Chapter 2) Once the UAV images were processed, they were input into ArcMap 10.6 and used as a basemap for digitizing trees in the riparian zone. The riparian zone, the zone between a stream and valley slopes influenced by flooding (Naiman and Decamps, 1997), was delineated using GPS surveys and alluvial soils (data from USDA, 2005; USDA, 2006). Once the riparian zone was defined, all standing trees were identified and marked as point features in their own shapefile. Damaged riparian trees were then digitized as line features and given the following attributes; condition (toppled, or uprooted), length, diameter, azimuth, and volume. The measuring tool in ArcMap 10.6 was used to obtain the length and diameter of each of the damaged trees (toppled or uprooted). Diameter was measured near the center of the visible portion of the damaged trees.

Results

Valley Cross-Section Comparison. The UAV DSM provided similar results to the field-surveyed cross-sections. The root mean square errors (RMSEs) of the valley cross-sections were relatively low and ranged from 0.15 m at Lick Branch to 1.82 m at Indian Creek and the differences could mostly be explained by vegetation. All but Indian Creek had RMSEs less than 0.52 m. Dry Creek (Fig. 12a and 12b), Lower Tabor Creek (Appendix), Upper Tabor Creek (Fig. 13a and 13b), and Lick Branch (Appendix) all had $R^2 > 0.92$ when comparing the survey data to the UAV DSM data. This shows that the UAV imagery can accurately represent landforms and morphologies of fluvial environments. Spring Branch had R^2 values of 0.79 and Indian Creek had R^2 values of 0.27 (Appendix). Spring Branch had lower R^2 values, because the thalweg

depths did not match between the UAV imagery and survey data. The cross-sections followed the same pattern at the same location across the valley, but the elevation data was shifted down for the UAV DSM since the thalweg depths for the UAV data were at a higher elevation than the survey data. It is unclear why there was poor correlation ($R^2 = 0.27$) between the two elevation datasets at Indian Creek, where the thalweg location across the valley bottom did not even match up (Appendix). Potential reasons for the error could be image processing and/or GCP configuration, although the latter is unlikely since the distribution of GCPs was similar across all the sites. Vegetation also affects the UAV DSM (Watanabe and Kawahari, 2016), the UAV DSM is a surface elevation model and does not always represent the ground elevation data. Some of the fluctuations in the UAV DSM data are because of vegetation.

Damaged Trees. Of the 121 damaged trees sampled (total for all sites) 48 were unable to be identified in the UAV imagery, this is because of canopy cover (71%), sediment deposition (13%), newly fallen/deposited since the UAV flight (8%), image processing (4%), and GPS accuracy (4%) (Table 11). Although one set of UAV imagery was taken during the leaf-off season (March 2018), branches from standing trees still blocked the view of damaged trees in the UAV imagery, this was considered canopy cover. Some of the trees recorded in the field were partially buried by sediment, and were unable to be detected when looking in the UAV imagery, this was considered as sediment deposition. In total, 73 damaged trees were able to be compared. Newly fallen trees were able to be identified because they can be seen in the UAV images as standing trees. Image processing prevented some of the damaged trees from being seen because the image processing software was unable to identify key points in the photos, resulting in blurred spots in the imagery (Fig. 14). This mostly occurred in the heavily forested areas where there were not distinguishing features that the software could identify. GPS accuracy averaged

from 1-3 m but could sometimes be less accurate. In some cases, the GPS point lay outside of the transect area on the UAV imagery and the damaged tree that the point corresponded to could not be identified.

Diameter Comparison. The regression analysis for diameter measurements between the UAV imagery and the total diameter and the UAV imagery and the sample diameter had R^2 values of 0.63 and 0.72, respectively, and both were statistically significant ($p < 0.01$). The total diameter measurement represents the measurement recorded in the field for the mid-point of the whole tree, while the sample diameter measurement represents the diameter measurement recorded at the mid-point within the 5 m wide sampling area. Further analysis of the UAV measurements found that the R^2 values for the total diameter and sample diameter were highest at Dry Creek and Lower Tabor Creek and lowest at Indian Creek and Lick Branch (Table 12). When the UAV measurement was compared to both the sample diameter and the total diameter measurement and preferentially chosen for the closest values, the R^2 value = 0.82 (Fig. 15).

Length Comparison. Of the 73 trees for which length could be measured, 34 were mostly visible. Of the blocked trees some were concealed by canopy cover, branches, and debris, others were buried by gravel or in jams of other trees, or were washed out as the same color as the surrounding gravel. The RMSE between length measurements for all trees was 2.25 m. The $R^2 = 0.41$ when comparing the field survey and UAV length measurements for all the trees. When comparing only mostly visible trees the R^2 value increased to 0.80 (Fig. 16). Dry Creek and Spring Branch had the highest R^2 values when comparing field measurements of tree length to the UAV measurement of tree length, while Indian Creek and Lick Branch had the lowest R^2 values (Table 12). By comparing only the mostly visible trees and excluding the two sites with the lowest R^2 values (Indian Creek and Lick Branch) the R^2 value increased to 0.86 (Fig. 17).

Volume Comparison. Volume of the damaged trees was estimated using the following equation, $V = \pi r^2 h$. Where r is the radius and h is the tree length. Volume was calculated from the field measurements and UAV measurements and then compared. The $R^2 = 0.37$ when comparing all the trees for which volume could be estimated (Fig. 18). However, when only comparing the damaged trees that are mostly visible in the UAV imagery R^2 increases to 0.75 (Fig. 19). Volume estimates from the UAV imagery were slightly worse ($R^2 = 0.75$), than estimates of diameter ($R^2 = 0.82$) and length ($R^2 = 0.86$). This is because in order to calculate the volume estimate both the diameter and length measurement were used. Thus small errors in diameter or length could cause errors in the volume estimate.

Discussion

Errors between UAV and field measurements of diameter were typically low (4 cm average) (Table 13). The largest differences between the field and the UAV measurements occurred at Indian Creek in which the largest difference between the total diameter measurement and the UAV measurement was 24 cm (Table 13) and 15 cm for the sample measurement (Table 14). However, both of these measurements were only 2 cm and 3 cm off from the other estimate, showing the variability in tree diameter and sample location. In total 90% of all the measurements were within 9 cm of each other, and 80% of the measurements were within 5 cm. There is also a correlation between the spatial resolution of the UAV imagery and the magnitude of measurement errors: as the spatial resolution decreases the absolute difference between measurements increase (Fig. 20).

Lick Branch and Indian Creek had low R^2 relationships between the field measurements and the UAV measurements because of the number of damaged trees that were fully or partially

obscured in the UAV imagery. The objects blocking the view of a damaged tree affected the location where the diameter was measured and often affected tree length measurements; Indian Creek and Lick Branch had 66% and 100% of the damaged trees partially blocked from view. The damaged trees were visible enough to derive measurements; however, the measurements were not representative of the whole tree.

Another reason for differences in the two methods of measuring length concerns the angles of damaged trees. If the tree was not flat on the ground, the angle of the tree will cause the tree length measured in the UAV imagery to differ from the actual tree length. The measured length on the UAV imagery would theoretically be shorter than the actual tree length, with error increasing with the angle of the tree off the ground level (Fig. 21). Although damaged trees were classified as toppled or uprooted in the field, the angle of the tree was not measured so this error could not be assessed.

Differences in UAV measurements also may not align with the field measurements because of GPS accuracy. Small changes in sampling location can result in changes to diameter. Comparing field sample measurements to field total measurements show that even on the same tree, diameter can fluctuate, thus if GPS accuracy varies finding the same sampling location on the imagery, can be impossible. The GPS accuracy in this study could get up to sub-meter accuracy, but averaged from 1-3 m. This accuracy range was generally sufficient enough to identify the damaged tree location, but not the exact location of the diameter measurement. It is important to note that field measurements may also contain errors, which was not evaluated in this study.

The use of UAVs for this study produced accurate quantification of landforms and damaged trees. RMSEs were lowest when comparing tree diameter and greatest when comparing

tree length. Measurement errors could mostly be explained by vegetation obscuring damaged tree measurements and ground surface elevations. However, the UAV measurements still provided results that were statistically the as field measurements. Additionally, using the UAV imagery greatly reduced time spent quantifying forest damage.

Conclusions

UAV imagery can be used to analyze riparian forest damage and fluvial landforms. This study found high R^2 values (> 0.90) at four of the six sites when comparing the UAV DSM data to field surveys of fluvial landforms. Additionally, R^2 values greater than 0.80 were obtained when comparing UAV and field measurements of damaged riparian tree diameter and length. Limits to UAV imagery and the data they can provide come from vegetation and other debris that can prevent or obscure measurements. Vegetation can cause differences in landform elevations and also limit accurate measurements of tree length and where measurements of tree diameter are taken (Table 11).

This study shows that UAV imagery can be a useful and accurate tool for assessing riparian forest flood damage and fluvial landforms. However more studies are needed to further reduce the effects of various errors on UAV measurements. The use of UAV data provides cost-effective, high-resolution data which can save time and money when conducting environmental assessments. Informally comparing field sampling time to UAV analysis, showed that using the UAV imagery to sample the same area as the field survey took at the most a quarter of the time (excluding image processing time). Field sampling along each transect took from one to two hours to collect the data on damaged tree location, diameter, length, azimuth, and condition (standing, toppled, uprooted). The UAV imagery in this study provided extremely useful data on

riparian forest damage from a large recurrence interval flood (>500-year) in a region lacking in understanding of the relationship between riparian vegetation and flooding.

Table 11. Sources and Explanations of Measurement Errors

Source of Error	Definition of Error	Occurrence (%)	Range of Effects
Canopy Cover	Damaged tree blocked by standing tree branches.	71	Prevented full tree lengths to be measured and limited where diameter measurement was taken.
Buried	Sediment deposition over damaged trees.	13	Prevented full tree diameter and lengths to be measured.
Newly Fallen/ Deposited	Tree damage that occurred after UAV imagery was collected.	8	Damaged trees volumes could not be calculated for trees that were still standing at the time of the UAV imagery acquisition.
Image Processing	Lack of unique features (tie points) in imagery resulted in blurred spots.	4	Prevented damaged tree location to be identified.
GPS Accuracy	Variability in GPS accuracy prohibited the identification of damaged tree location.	4	Prevented damaged tree location to be identified.

Table 12. Comparison of UAV and Field Measurements of Diameter and Length

		R^2 Value		
Site	Sample Size	Diameter UAV vs Sample	Diameter UAV vs Total	Length UAV vs Field
Dry Creek	7	0.91	0.89	0.79
Indian Creek	24	0.64	0.32	0.26
Lower Tabor Creek	18	0.81	0.81	0.40
Upper Tabor Creek	8	0.62	0.65	0.34
Spring Branch	12	0.77	0.65	0.57
Lick Branch	4	0.06	0.60	0.01
All Sites	73	0.72	0.63	0.41

*Two measurements of diameter were taken in the field, "Sample" refers to the diameter measurement taken within the five meter wide sampling transect, "Total" refers to the diameter measurement recorded for the whole tree.

Table 13. Differences between Field Survey "Total" and UAV Diameter Measurements

Site	Average	Smallest	Largest	Median	UAV Imagery Resolution
Dry Creek	0.02	0.00	0.04	0.01	0.05
Indian Creek	0.03	0.00	0.24	0.02	0.05
Lower Tabor Creek	0.03	0.00	0.13	0.02	0.04
Upper Tabor Creek	0.03	0.01	0.06	0.03	0.03
Spring Branch	0.05	0.01	0.09	0.04	0.03
Lick Branch	0.09	0.03	0.13	0.09	0.08
All Sites	0.04	0.00	0.24	0.03	0.03-0.08

Table 14. Differences between Field Survey "Sample" and UAV Diameter Measurements (m)

Site	Average	Smallest	Largest	Median	UAV Imagery Resolution
Dry Creek	0.04	0.00	0.04	0.01	0.05
Indian Creek	0.03	0.00	0.15	0.01	0.05
Lower Tabor Creek	0.04	0.00	0.10	0.03	0.04
Upper Tabor Creek	0.04	0.01	0.08	0.02	0.03
Spring Branch	0.04	0.00	0.10	0.04	0.03
Lick Branch	0.09	0.03	0.13	0.09	0.08
All Sites	0.03	0.00	0.15	0.02	0.03-0.08

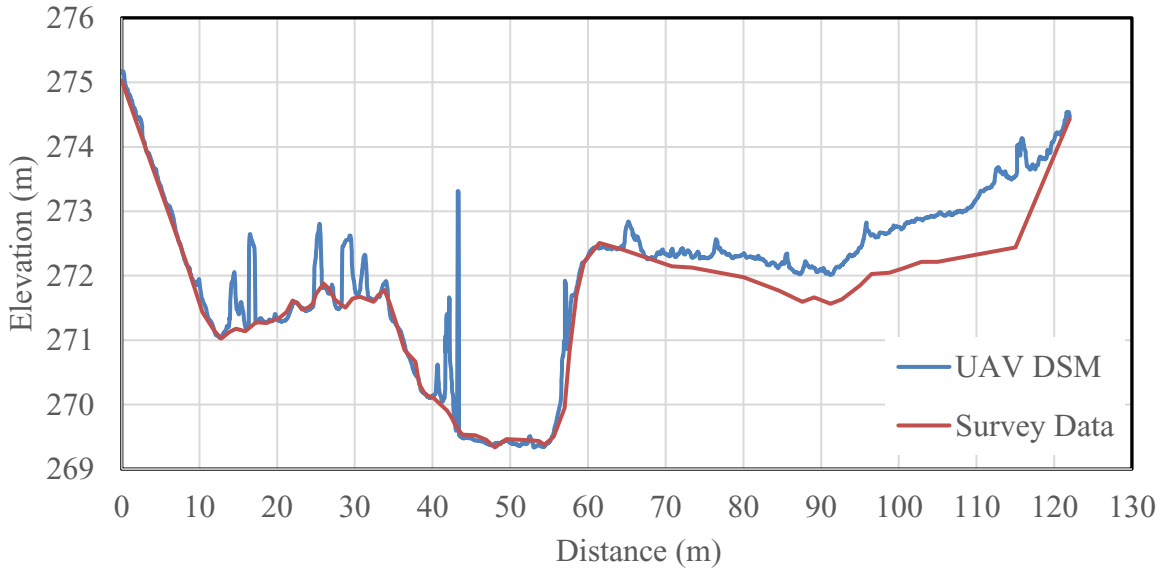

Fig. 12a. Cross-Section of Dry Creek using UAV DSM and Survey Data

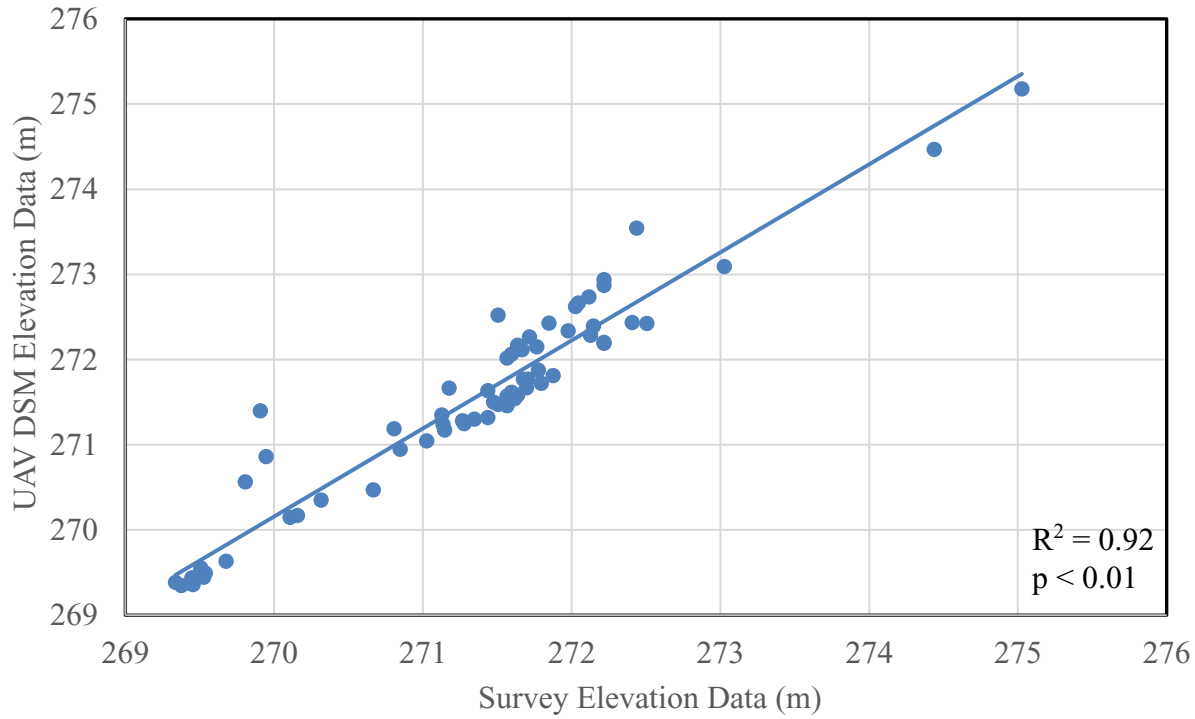

Fig. 12b. Regression Analysis of UAV DSM and Survey Elevation Data at Dry Creek

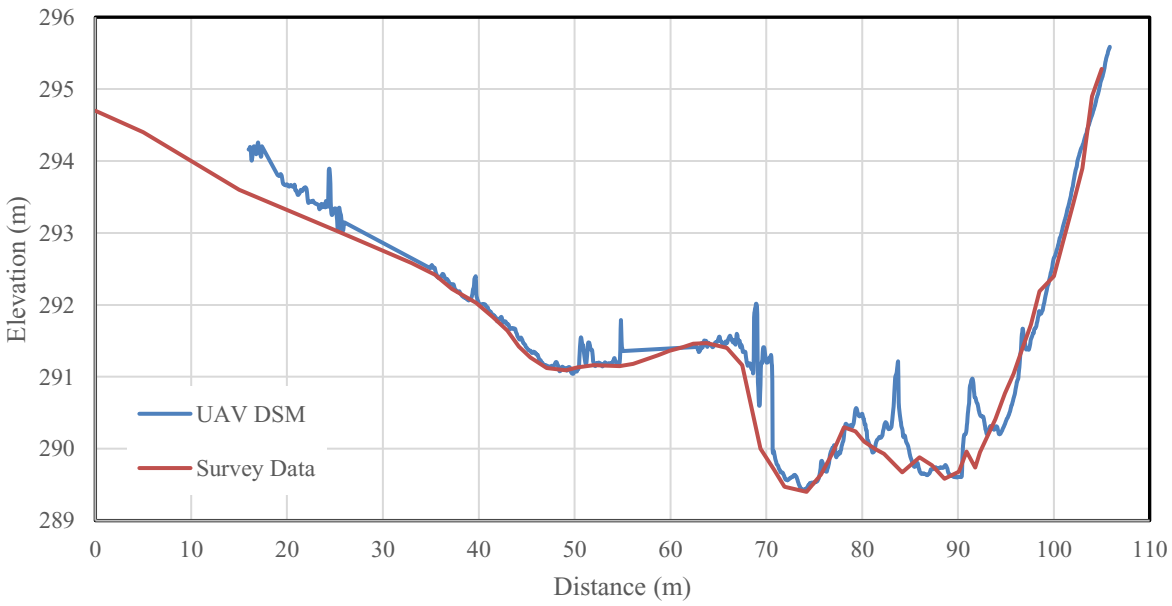

Fig. 13a. Cross-Section of Upper Tabor Creek using UAV DSM and Survey Data

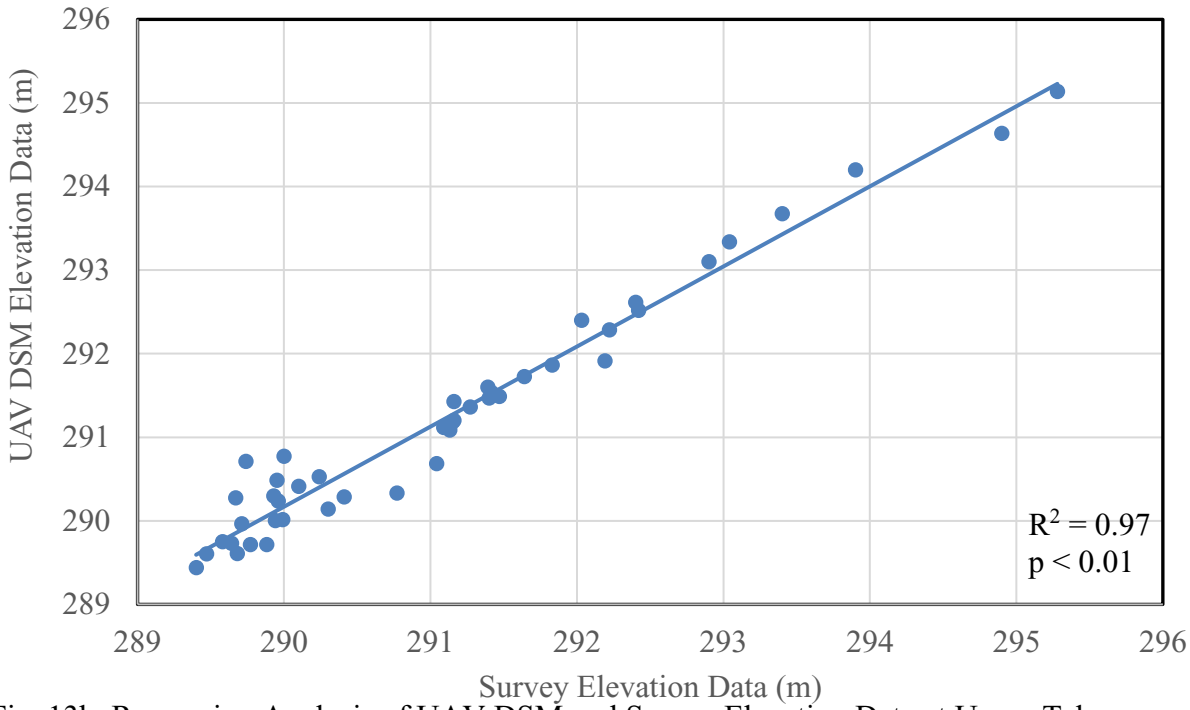

Fig. 13b. Regression Analysis of UAV DSM and Survey Elevation Data at Upper Tabor Creek

Fig. 14. Blurred Spots on the UAV Imagery from the Image Processing

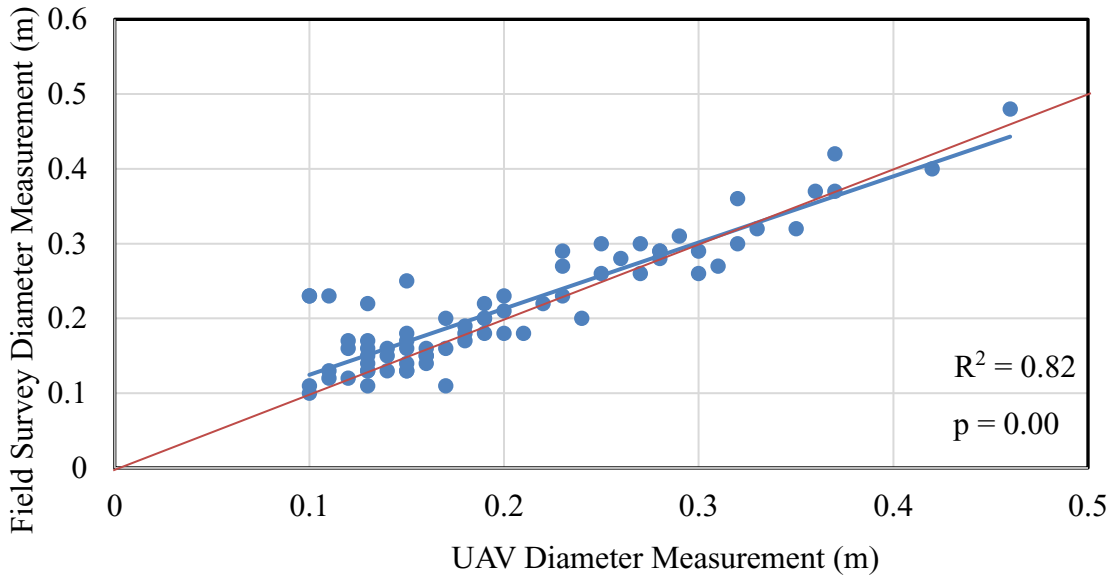

Fig. 15. Preferentially Chosen Survey Diameter Compared to UAV Diameter Measurement

*Two diameter measurements were taken in the field, for this figure the diameter measurement which was closest to the UAV diameter measurement was compared with the UAV measurement.

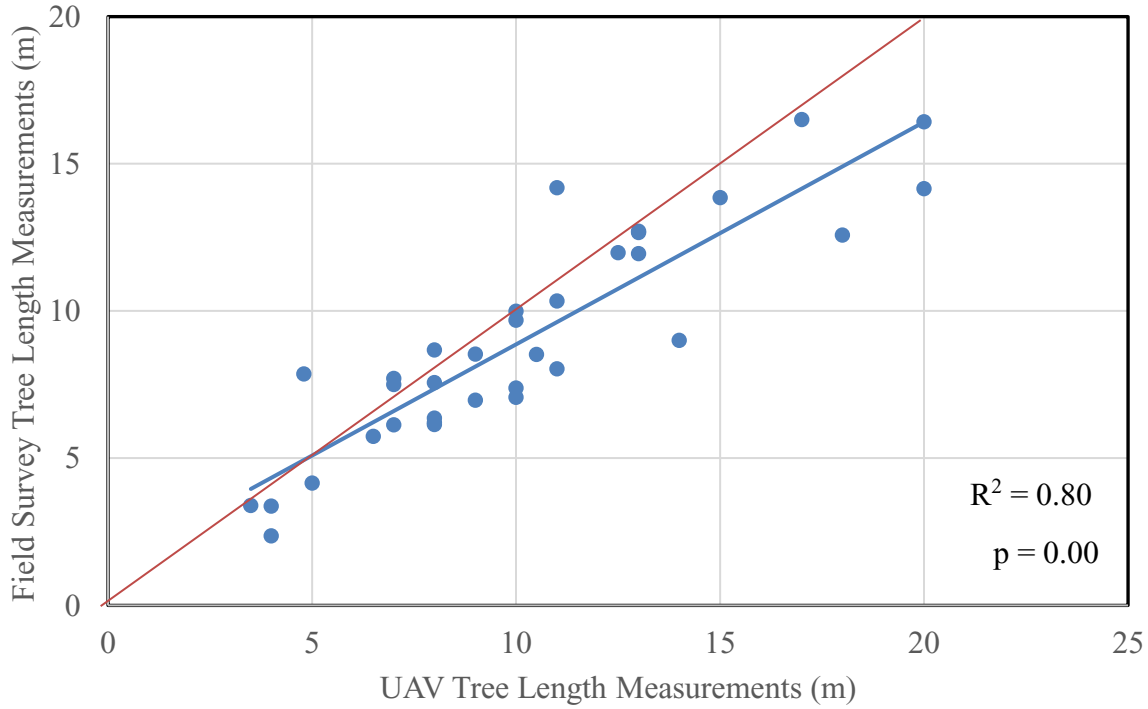

Fig. 16. Field Survey Compared to UAV Tree Length Measurements using only Mostly Visible Trees

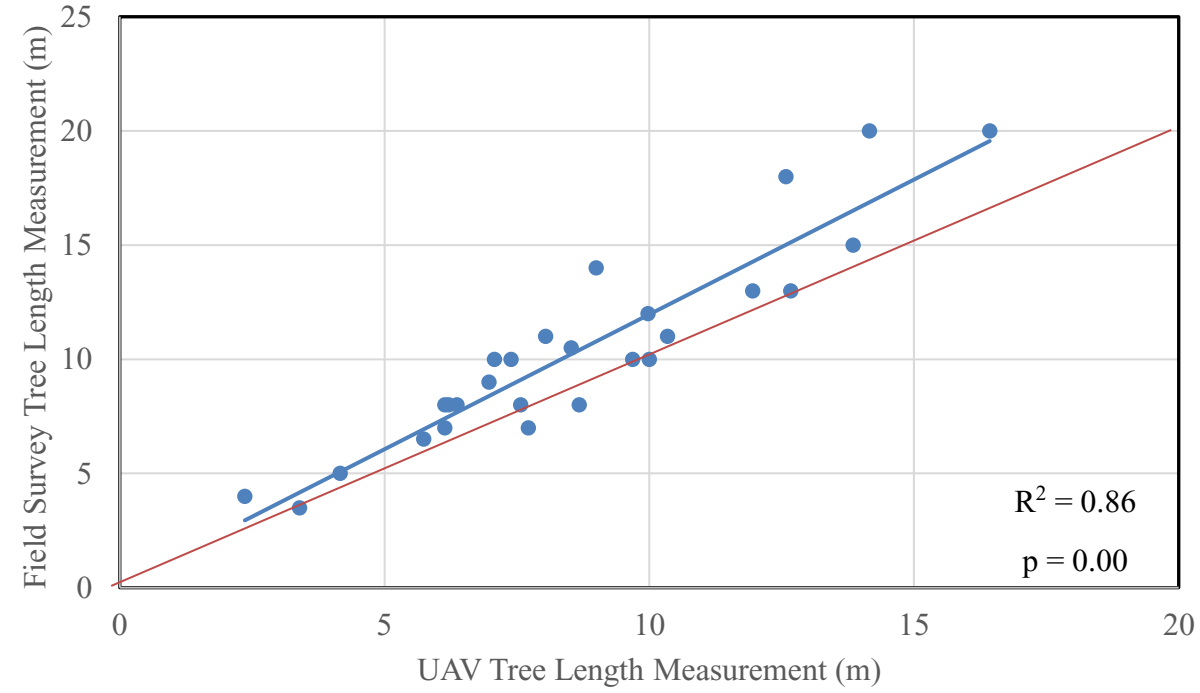

Fig. 17. Field Survey Compared to UAV Tree Length Measurements using only Mostly Visible Trees and Excluding Indian Creek and Lick Branch

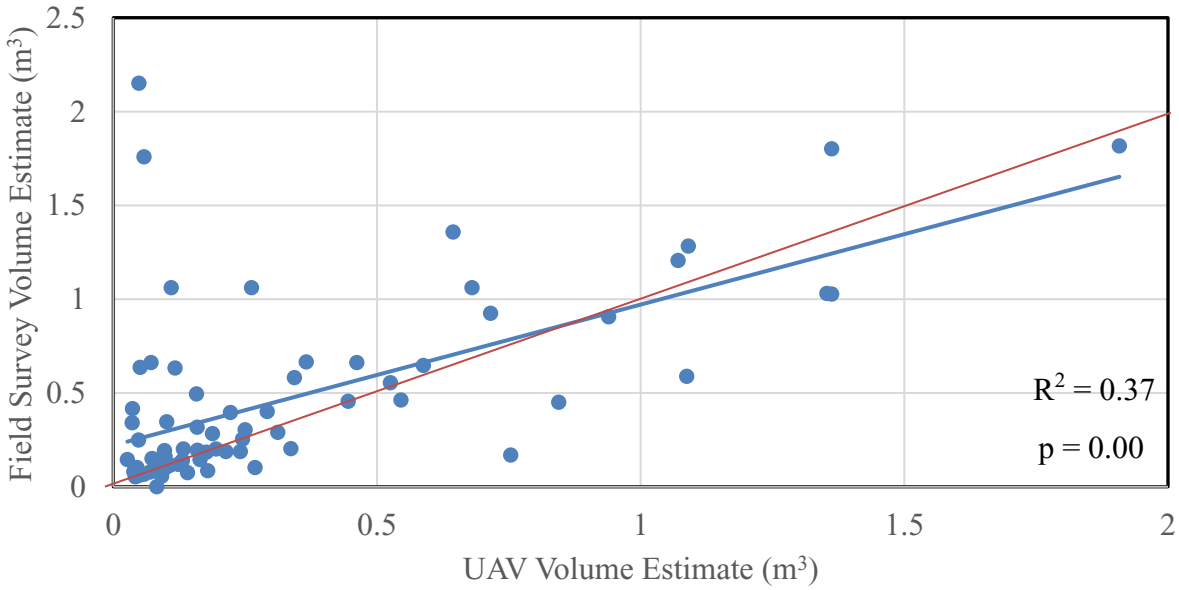

Fig. 18. Field Survey Compared to UAV Volume Estimates (All Trees)

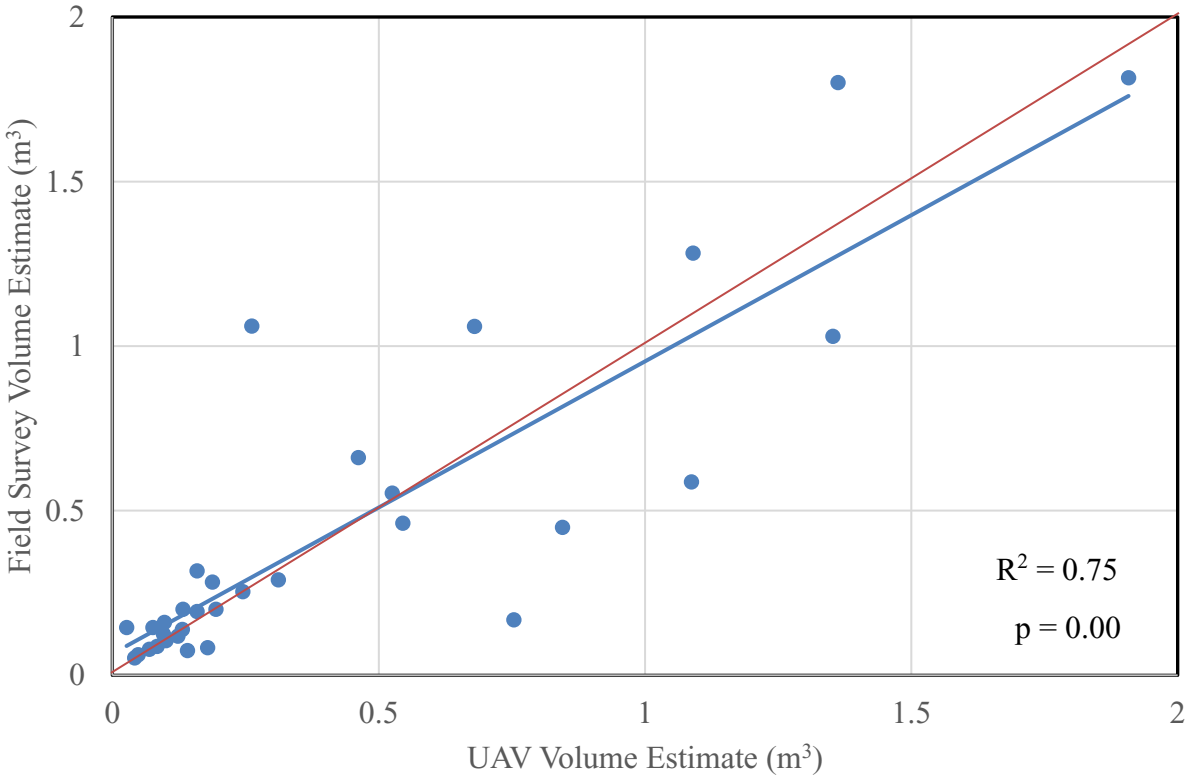

Fig. 19. Field Survey Compared to UAV Volume Estimates Including only Mostly Visible Trees

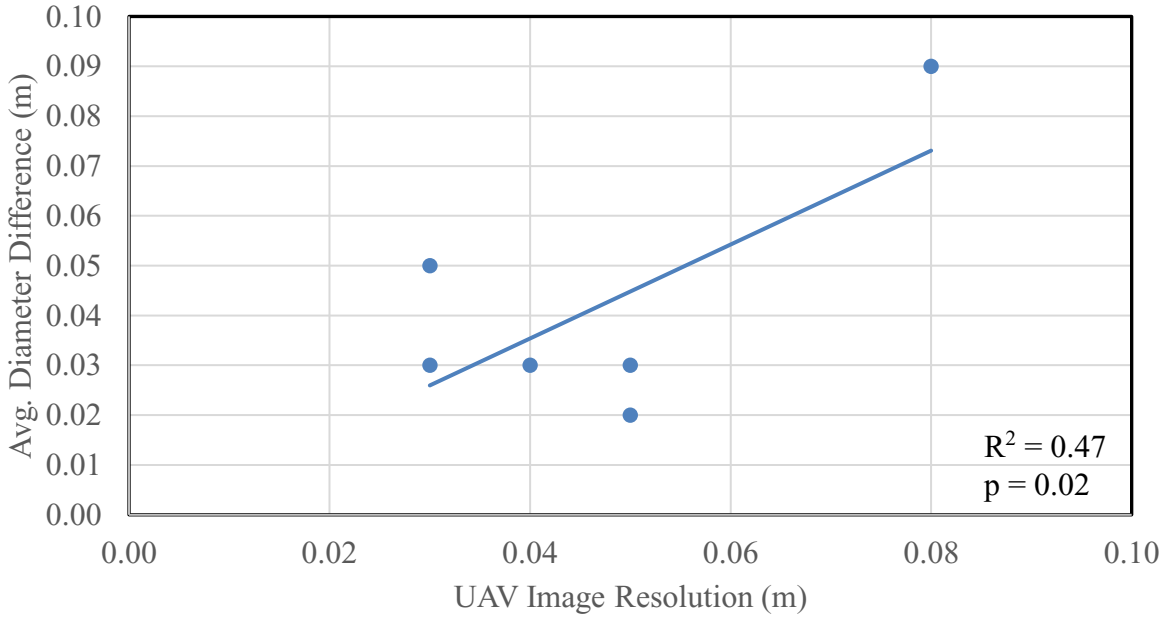

Fig. 20. Relationship Between Image Resolution and Measurement Errors of Diameter

Fig. 21. Toppled Tree Length Underestimated in UAV Imagery. Terrestrial Photograph (left) and UAV Imagery (right) of the Same Tree

CHAPTER FOUR: CONCLUSION

This study contributes to our understanding of the applications and limitations of using UAVs in environmental assessment, the relationship between riparian forests and flooding, and the effects of climate change. High-resolution UAV imagery was used to estimate riparian forest damage following a >500 year flood in the North Fork of the White River watershed in the Missouri Ozarks. Individual tree volume estimates and canopy loss were calculated from UAV imagery to quantify the forest damage. The measurements derived from the UAV imagery were then compared to field measurements. Once the riparian forest damage was quantified and identified across fluvial landforms, it was compared to hydrologic and morphologic variables.

UAV imagery can be used to derive accurate measurements of damaged tree diameter and length. Measurements derived from the UAV imagery were statistically the same as field measurements. However, there are limitations to using this data. One can only measure what is visible in the imagery. Thus if there is anything above the damaged tree, blocking it from view, the measurements may be skewed (i.e., length shortened or diameter changed). Canopy cover, debris jams, and branches all limit measurements derived from the imagery. UAV imagery can also be used to successfully create highly detailed and accurate topographic cross-sections of fluvial environments and landforms. The results in this study showed greater than 0.90 R^2 values at four out of the six sites when comparing UAV and field survey elevation data.. Additionally, the UAV imagery greatly reduced sampling time of forest damage, many times sampling time was reduced by at least 75%.

Stream power (mean and cross-sectional), confinement, sinuosity, and sediment size all had positive correlations with riparian forest damage. Cross-sectional stream power explained

the greatest percentage of the variance in total damaged tree volume and canopy loss. Riparian forest damage peaked at Lower Tabor Creek which had the greatest percentage of canopy loss, the greatest number of damaged trees, and the greatest volume of damaged trees. The greatest riparian forest damage at Lower Tabor Creek can be explained by the fact that, compared to the other sites, it was the most sinuous and confined, had the greatest bankfull width, slope, and mean stream power. However, Dry Creek had the greatest density of damaged riparian trees per hectare of valley floor. Additionally, forest damage tended to be greatest in reaches with the largest drainage areas. At all the sites, damaged riparian trees generally aligned with the main channel or chute flow direction and were not in jams. Jams were only present between the main channel and chutes and on the outside of channel bends.

This study presents data that can help better assess and predict ecological disturbances in riparian forests, such as extreme flooding, and can be used to support land management practices in Mark Twain National Forest in southern Missouri. UAVs can be a useful tool for monitoring forests and more efforts should be made to optimize image collection and processing procedures to improve UAV applicability and precision. Few studies have previously reported on the relationship among riparian forest, large woody debris, and large floods in the Ozarks, and across the Midwest. This study contributes to our understanding of how floods impact riparian forests in relationship to geomorphic variables. Increased flood risks due to climate change, may increase the demand for more studies in the future.

CHAPTER FIVE: REFERENCES

Agisoft Metashape., 2019. https://www.agisoft.com/. Accessed 20 January 2019.

Alexander, T.W., Wilson, G.L., 1995. Technique for estimating the 2- to 500-year flood discharges on unregulated streams in rural Missouri. Water-Resources Investigations Report 95, 1–33

Allen, M.S., Thapa, V., Arévalo, J.R., Palmer, M.W., 2012. Windstorm damage and forest recovery: accelerated succession, stand structure, and spatial pattern over 25 years in two Minnesota forests. Plant Ecology 213, 1833–1842.

Anderson, K., Gaston, K.J., 2013. Lightweight unmanned aerial vehicles will revolutionize spatial ecology. Frontiers in Ecology and the Environment 11, 138–146.

Andréasson, J., Bergström, S., Carlsson, B., Lindström, G., Graham, L.P., 2004. Hydrological change: climate change impact simulations for Sweden. Swedish Regional Climate Modelling Programme 33, 228–234.

Andresen, J., S. Hilberg, K. Kunkel, 2012: Historical climate and climate trends in the Midwestern USA. In: U.S. National Climate Assessment Midwest Technical Input Report.

Bendix, J., 1994. Scale, direction, and pattern in riparian vegetation-environment relationships. Annals of the Association of American Geographers 84, 652–665.

Bendix, J., 1997. Flood disturbance and the distribution of riparian species diversity. Geographical Review 87, 468.

Bendix, J., 1998. Impact of a flood on southern California riparian vegetation. Physical Geography 19, 162–174.

Bendix, J., 1999. Stream power influence on southern Californian riparian vegetation. Journal of Vegetation Science 10, 243–252.

Bendix, J., Hupp, C.R., 2000. Hydrological and geomorphological impacts on riparian plant communities. Hydrological Processes 14, 2977–2990.

Benke, A.C., Chaubey, I., Ward, G.M., Dunn, E.L., 2000. Flood pulse dynamics of an unregulated river floodplain in the southeastern U.S. coastal plain. Ecology 81, 2730.

Blizzard, E.M., Henken, D., Kabrick, J.M., Dey, D.C., Larsen, D.R., and Gwaze D., 2007, Shortleaf pine reproduction abundance and growth in pine-oak stands in the Missouri Ozarks: Proceedings of Shortleaf pine restoration and ecology in the Ozarks: U.S. Department of Agriculture, Forest Service, Northern Research Station, p. 138-146.

Borga, M., Stoffel, M., Marchi, L., Marra, F., Jakob, M., 2014. Hydrogeomorphic response to extreme rainfall in headwater systems: flash floods and debris flows. Journal of Hydrology 518, 194–205.

Brewer, C.W., Linnartz, N.E., 1973. The recovery of hurricane-bent loblolly pine. Louisiana State University Forestry Note 104. Louisiana State University, Baton Rouge.

Bull, W.B., 1979. Threshold of critical power in streams: discussion and reply. Geological Society of America Bulletin 90, 453–464.

Chandler, J., Ashmore, P., Paola, C., Gooch, M., Varkaris, F., 2002. Monitoring river-channel change using terrestrial oblique digital imagery and automated digital photogrammetry. Annals of the Association of American Geographers 92, 631–64

Chang, H., Knight, C.G., Staneva, M.P., Kostov, D., 2002. Water resource impacts of climate change in southwestern Bulgaria. GeoJournal 57, 159–168.

Chow, V.T., 1959. Open-channel hydraulics. Blackburn Press, Caldwell, NJ.

Costa, J.E., 1983. Paleohydraulic reconstruction of flash-flood peaks from boulder deposits in the Colorado Front Range. Geological Society of America Bulletin 94, 986–1004.

Dandois, J.P., Ellis, E.C., 2010. Remote sensing of vegetation structure using computer vision. Remote Sensing 2, 1157–1176.

Dandois, J., Olano, M., Ellis, E., 2015. Optimal altitude, overlap, and weather conditions for computer vision UAV estimates of forest structure. Remote Sensing 7, 13895–13920.

DJI., 2019. https://www.dji.com/phantom-4-pro/info#specs. Accessed 20 January 2019.

Duley, J.W., Boswell, C., Prewett, J., 2015. Recharge area of selected large springs in the Ozarks. Sinkholes and the Engineering and Environmental Impacts of Karst: Proceedings of the Fourteenth Multidisciplinary Conference.

Engelhardt, B.M., Weisberg, P.J., Chambers, J.C., 2011. Influences of watershed geomorphology on extent and composition of riparian vegetation. Journal of Vegetation Science 23, 127–139.

Erdman, J., 2017. Record flooding in April/May 2017 swamps parts of Missouri, Arkansas, Illinois. The Weather Channel.

Everham, E.M., Brokaw, N.V.L., 1996. Forest damage and recovery from catastrophic wind. Botanical Review 62, 113–185.

Everitt, J.H., Yang, C., Judd, F.W., Summy, K.R., 2010. Use of archive aerial photography for monitoring black mangrove populations. Journal of Coastal Research 264, 649–653.

Fierke, M.K., Kauffman, J.B., 2006. Riverscape-level patterns of riparian plant diversity along a successional gradient, Willamette river, Oregon. Plant Ecology 185, 85–95.

Fonstad, M.A., Dietrich, J.T., Courville, B.C., Jensen, J.L., Carbonneau, P.E., 2013. Topographic structure from motion: a new development in photogrammetric measurement. Earth Surface Processes and Landforms 38, 421–430.

Foreman, A.T., 2014, Climate change influence on historical flood variability in Ozark Highland Rivers, [M.S. Thesis]: Missouri State University.

Friedman, J.M., Lee, V.J., 2002. Extreme floods, channel change, and riparian forests along ephemeral streams. Ecological Monographs 72, 409-425.

Fryirs, K.A., Wheaton, J.M., Brierley, G.J., 2016. An approach for measuring confinement and assessing the influence of valley setting on river forms and processes. Earth Surface Processes and Landforms 41, 701–710.

Fujita, T., Itaya, A., Miura, M., Manabe, T., Yamamoto, S., 2003. Canopy structure in a temperate old-growth evergreen forest analyzed by using aerial photographs. Plant Ecology 168, 23–29.

Fuller, I.C., 2007. Geomorphic work during a “150-year” storm: contrasting behaviors of river channels in a New Zealand catchment. Annals of the Association of American Geographers 97, 665–676

Fuller, I.C., 2008. Geomorphic impacts of a 100-year flood: Kiwitea Stream, Manawatu catchment, New Zealand. Geomorphology 98, 84–95.

Garssen, A.G., Baattrup-Pedersen, A., Riis, T., Raven, B.M., Hoffman, C.C., Verhoeven, J.T.A., Soons, M.B., 2017. Effects of increased flooding on riparian vegetation: Field experiments simulating climate change along five European lowland streams. Global Change Biology 23, 1–12.

Getzin, S., Wiegand, K., Schöning, I., 2012. Assessing biodiversity in forests using very high-resolution images and unmanned aerial vehicles. Methods in Ecology and Evolution 3, 397–404.

Graf, W.L., 1983. Downstream changes in stream power in the Henry Mountains, Utah. Annals of the Association of American Geographers 73, 373–387.

Gran, K., Paola, C., 2001. Riparian vegetation controls on braided stream dynamics. Water Resources Research 37, 3275–3283

Gurnell, A.M., Piegay, H., Swanson, F.J., Gregory, S.V., 2002. Large wood and fluvial processes. Freshwater Biology 47, 601–619.

Harris, R.R., 1987. Occurrence of vegetation on geomorphic surfaces in the active floodplain of a California alluvial stream. American Midland Naturalist 118, 393.

Harrison, L.R., Dunne, T., Fisher, G.B., 2015. Hydraulic and geomorphic processes in an overbank flood along a meandering, gravel-bed river: implications for chute formation. Earth Surface Processes and Landforms 40, 1239–1253.

Heimann, D.C., Holmes, R.R., Harris, T.E., 2018. Flooding in the southern midwestern United States, April–May 2017. Open-File Report.

Hostens, D.S., 2019, Determining the effect of mission design and point cloud filtering on the quality and accuracy of SfM photogrammetric products derived from sUAS imagery, [M.S. Thesis]: Missouri State University.

Hupp, C.R., Bornette, G., 2005. Vegetation as a tool in the interpretation of fluvial geomorphic processes and landforms in humid temperate areas. Tools in Fluvial Geomorphology 269–288

Hupp, C.R., Osterkamp, W.R., 1996. Riparian vegetation and fluvial geomorphic processes. Geomorphology 14, 277–295.

Intelisolve, 2006. Hydraflow Express User Manual, 0-106

Jacobson, R.B., Primm, A.T., 1997. Historical land-use changes and potential effects on stream disturbance in the Ozarks Plateaus, Missouri. United States Geological Survey Water-Supply Paper 2484, 1–85.

Jacobson, R.B., Gran, K.B., 1999. Gravel sediment routing from widespread, low- intensity landscape disturbance, Current River Basin, Missouri. Earth Surface Processes and Landforms 24, 897–917.

Jeong, E., Park, J.-Y., Hwang, C.-S., 2018. Assessment of UAV photogrammetric mapping accuracy in the beach environment. Journal of Coastal Research 85, 176–180.

Johnson, S.L., Swanson, F.J., Grant, G.E., Wondzell, S.M., 2000. Riparian forest disturbances by a mountain flood — the influence of floated wood. Hydrological Processes 14, 3031–3050.

Katz, G.L., Friedman, J.M., Beatty, S.W., 2005. Delayed effects of flood control on a flood-dependent riparian forest. Ecological Applications 15, 1019–1035.

Klemas, V., 2015. Remote sensing of floods and flood-prone areas: an overview. Journal of Coastal Research 314, 1005–1013.

Kozlowski, T.T., 2002. Physiological-ecological impacts of flooding on riparian forest ecosystems. Wetlands 22, 550–561.

Kupfer, J.A., Myers, A.T., Mclane, S.E., Melton, G.N., 2008. Patterns of forest damage in a southern Mississippi landscape caused by Hurricane Katrina. Ecosystems 11, 45–60.

Lecce, S.A., 1997. Nonlinear downstream changes in stream power on Wisconsins Blue River. Annals of the Association of American Geographers 87, 471–486.

Leopold, L.B., Wolman, M.G., 1957. River channel patterns: braided, meandering, and straight. US Geological Survey Professional Paper 282-B

Lyon, J., Sagers, C.L., 1998. Structure of herbaceous plant assemblages in a forested riparian landscape. Plant Ecology 138, 1–16.

Martin, D.J., Pavlowsky, R.T., 2011. Spatial patterns of channel instability along an Ozark river, Southwest Missouri. Physical Geography 32, 445–468.

Martin, D.J., Harden, C.P., Tran, L., Pavlowsky, R.T., 2018. Investigating patterns of in-channel wood deposition locations in a low-gradient, variably-confined alluvial river system. Progress in Physical Geography 42, 139–161.

Mckenney, R., Jacobson, R.B., Wertheimer, R.C., 1995. Woody vegetation and channel morphogenesis in low-gradient, gravel-bed streams in the Ozark Plateaus, Missouri and Arkansas. Geomorphology 13, 175–198.

Miller, S.M., Wilkerson, T.F., 2001. North Fork River watershed inventory and assessment, Missouri Department of Conservation.

Morche, David, et al. “Hydrology and geomorphic effects of a high-magnitude flood in an alpine river.” *Geografiska Annaler: Series A, Physical Geography*, vol. 89, no. 1, 2007, pp. 5–19.

MRCC, 2019. https://mrcc.illinois.edu/CLIMATE/Station/Annual/StnAnnual BTD2.jsp. Accessed 12 January 2019.

MRLC, 2016. https://www.mrlc.gov/national-land-cover-database-nlcd-2016. Accessed 09 January 2019.

Murphy, M.L., Koski, K.V., 1989. Input and depletion of woody debris in Alaska streams and implications for streamside management. North American Journal of Fisheries Management 9, 427–436.

Nagel, D.E., Buffington, J.M., Parkes, S.L., Wenger, S., Goode, J.R., 2014. A landscape scale valley confinement algorithm: delineating unconfined valley bottoms for geomorphic, aquatic, and riparian applications.

Nakamura, F., Swanson, F.J., 1994. Distribution of coarse woody debris in a mountain stream, western Cascade Range, Oregon. Canadian Journal of Forest Research 24, 2395–2403.

Naiman, R.J., Decamps, H., 1997. The ecology of interfaces: riparian zones. Annual Review of Ecology and Systematics 28, 621–658.

Pavlowsky, R.T., Owen, M.R., Bradley, R.A., 2016. Recent increase in extreme rainfall amounts in the Big Barren Creek Watershed, S.E. Missouri. Missouri Natural Areas Newsletter 16, 19–24.

Phillips, J.D., 2002. Geomorphic impacts of flash flooding in a forested headwater basin. Journal of Hydrology 269, 236–250.

Piégay, H., Marston, R.A., 1998. Distribution of large woody debris along the outer bend of meanders in the Ain River, France. Physical Geography 19, 318–340.

Poff, N.L., Tokar, S., Johnson, P., 1996. Stream hydrological and ecological responses to climate change assessed with an artificial neural network. Limnology and Oceanography 41, 857–863.

Pryor, S.C., Scavia, D., Downer, C., Gaden, M., Iverson, L., Nordstrom, R., Patz, J., Robertson, G.P., 2014. Ch. 18: Midwest. Climate change impacts in the United States: the third national climate assessment.

Quilter, M., Anderson, V., 2000. Low altitude/large scale aerial photographs: a tool for range and resource managers. Rangelands 22, 13–17.

Raeker, G.W., Moser, K., Butler, B.J., Fleming, J., Gormanson, D.D., Hansen, M.H., Kurtz, C.M., Miles, P.D., Morris, M., Treiman, T.B., 2010. Missouri's forests 2008. Resource Bulletin. NRS-54

Rosgen, D., 1996. Applied river morphology. Wildland Hydrology, Pagosa Springs, Colorado.

Sauer, C.O., 1920. The geography of the Ozark Highland of Missouri. The University of Chicago Press, Chicago, IL.

Shepherd, S.L., Dixon, J.C., Davis, R.K., Feinstein, R., 2010. The effect of land use on channel geometry and sediment distribution in gravel mantled bedrock streams, Illinois River watershed, Arkansas. River Research and Applications.

Stambaugh, M.C., Muzika, R.M., Guyette, R.P., 2002. Disturbance characteristics and overstory composition of an old-growth shortleaf pine (Pinus echinata) forest in the Ozark Highlands, Missouri, USA. Natural Areas Journal 22, 108–119.

Steele, K.L., Kabrick, J.M., Dey, D.C., Jensen, R.G., 2013. Restoring riparian forests in the Missouri Ozarks. Northern Journal of Applied Forestry 30, 109–117.

Stephens, S.L., Fry, D.L., Franco-Vizcaíno, E., 2008. Wildfire and spatial patterns in forests in northwestern Mexico: the United States wishes it had similar fire problems. Ecology and Society 13.

Swanson, F.J., Johnson, S.L., Gregory, S.V., Acker, S.A., 1998. Flood disturbance in a forested mountain landscape. BioScience 48, 681–689.

Tal, M., Gran, K., Murray, A.B., Paola, C., Hicks, D.M., 2004. Riparian vegetation as a primary control on channel characteristics in multi-thread rivers. Riparian Vegetation and Fluvial Geomorphology Water Science and Application 43–58

United States Department of Agriculture (USDA), 2005. Soil survey of Douglas County, Missouri. National Cooperative Soil Survey.

United States Department of Agriculture (USDA), 2006. Soil survey of Howell County, Missouri. National Cooperative Soil Survey.

US Department of Commerce, NOAA, National Weather Service, 2017. Historic flooding event -- 28-30 April 2017. National Weather Service

Vanlooy, J.A., Martin, C.W., 2005. Channel and vegetation change on the Cimarron River, southwestern Kansas, 1953–2001. Annals of the Association of American Geographers 95, 727–739.

Watanabe, Y., Kawahara, Y., 2016. UAV photogrammetry for monitoring changes in river topography and vegetation. Procedia Engineering 154, 317–325.

Warrick, J.A., Ritchie, A.C., Adelman, G., Adelman, K., Limber, P.W., 2017. New techniques to measure cliff change from historical oblique aerial photographs and structure-from-motion photogrammetry. Journal of Coastal Research 331, 39–55.

Wohl, E., Cadol, D., 2011. Neighborhood matters: patterns and controls on wood distribution in old-growth forest streams of the Colorado Front Range, USA. Geomorphology 125, 132–146

Wolman, M.G., 1954. A method of sampling coarse river-bed material. Transactions, American Geophysical Union 35, 951.

Zahawi, R.A., Dandois, J.P., Holl, K.D., Nadwodny, D., Reid, J.L., Ellis, E.C., 2015. Using lightweight unmanned aerial vehicles to monitor tropical forest recovery. Biological Conservation 186, 287–29

CHAPTER SIX: APPENDIX

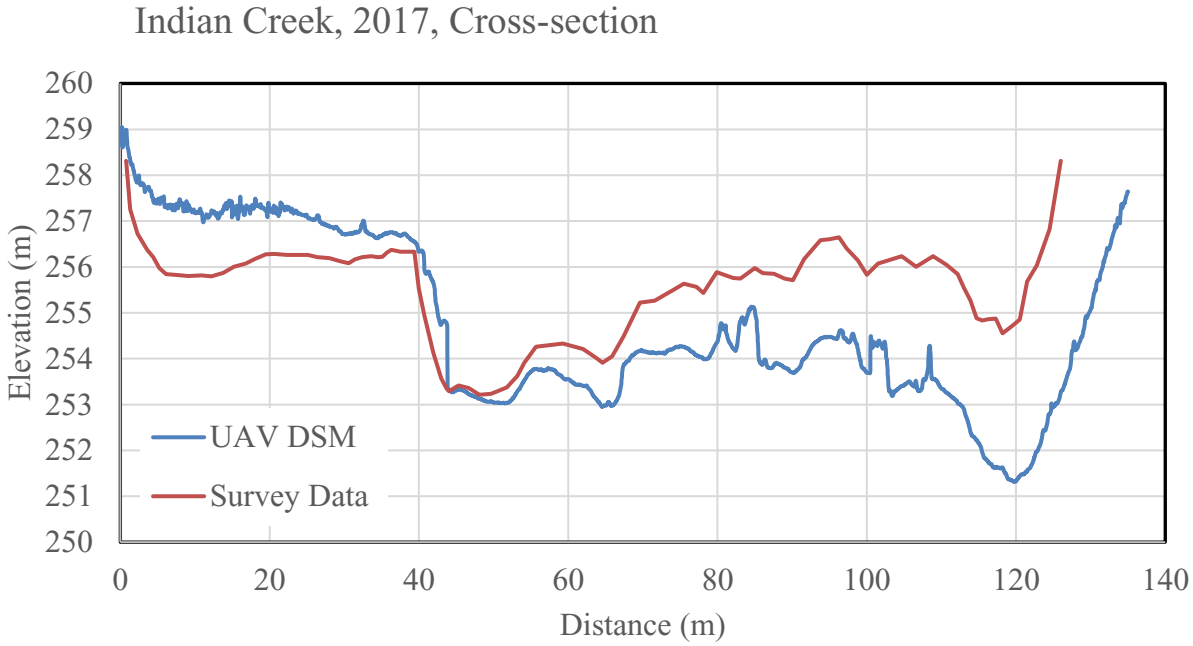

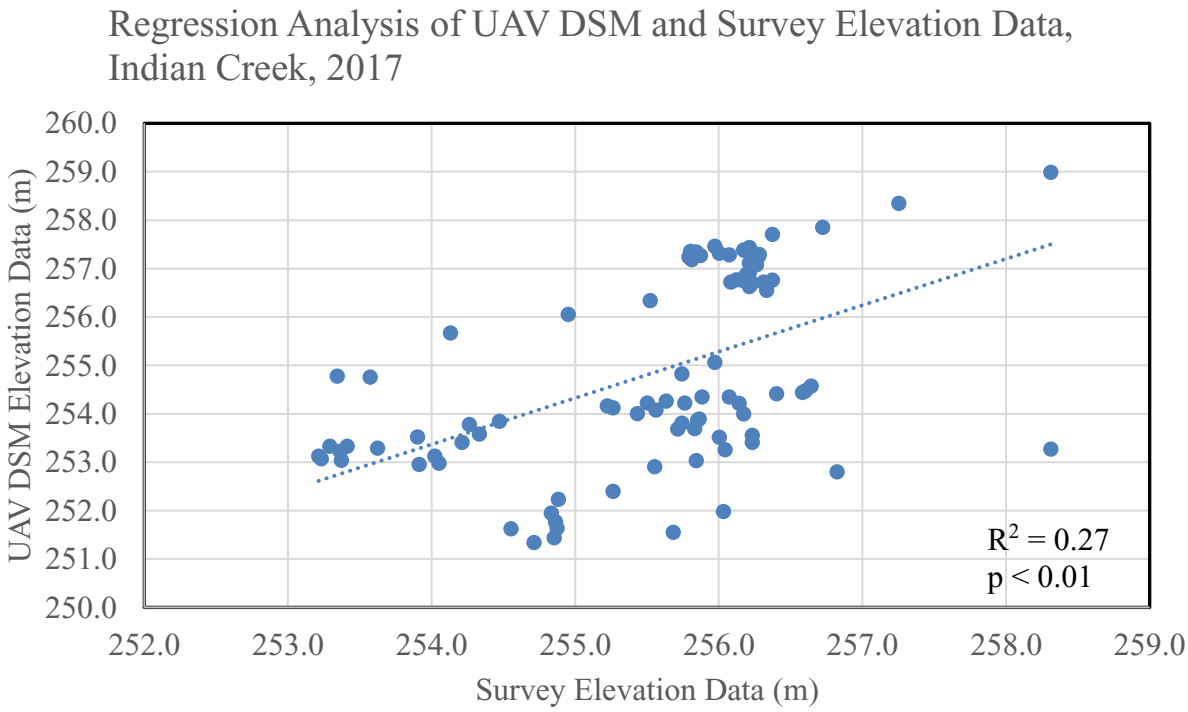

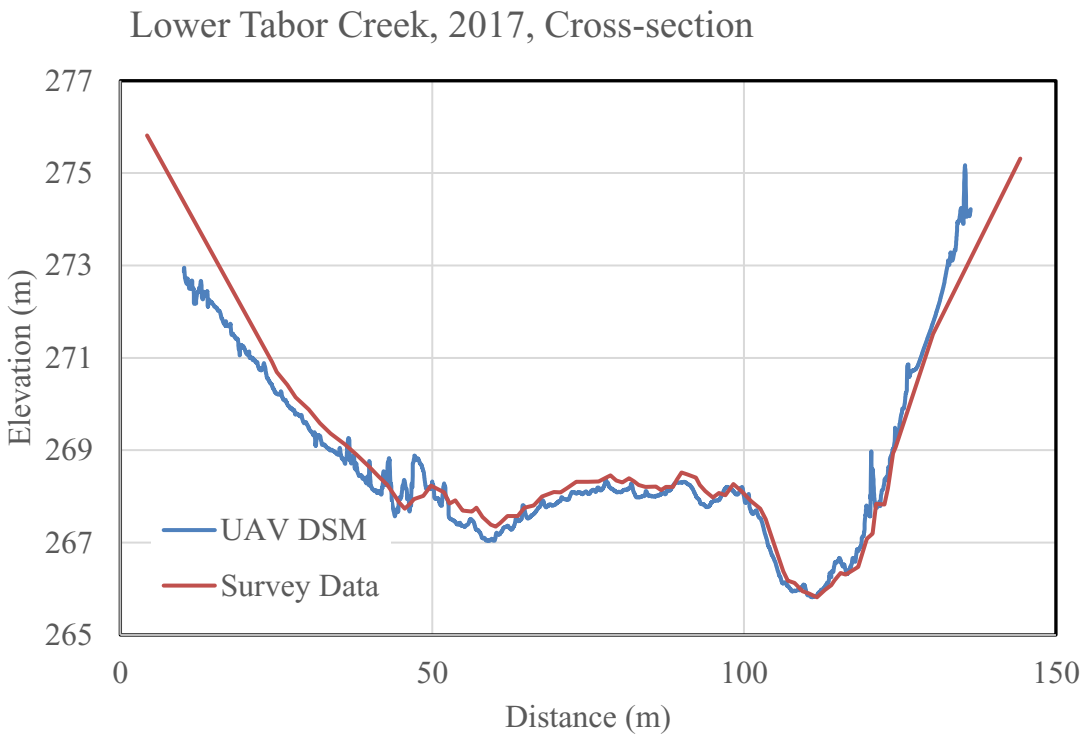
Lower Tabor Creek, 2017, Cross-section
277
275
273
271
269
267
265
Elevation (m)
UAV DSM
Survey Data
0
50
100
150
Distance (m)

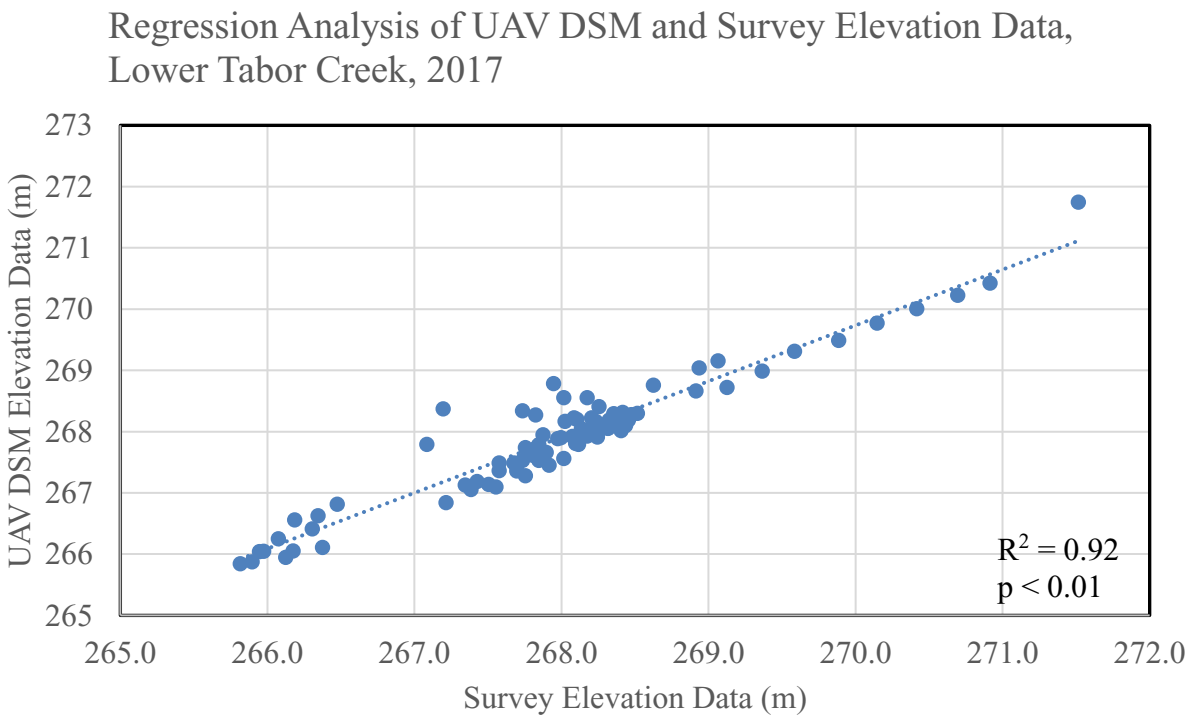
Regression Analysis of UAV DSM and Survey Elevation Data, Lower Tabor Creek, 2017
273
272
271
270
269
268
267
266
265
UAV DSM Elevation Data (m)
R2 = 0.92
p < 0.01
265.0
266.0
267.0
268.0
269.0
270.0
271.0
272.0
Survey Elevation Data (m)

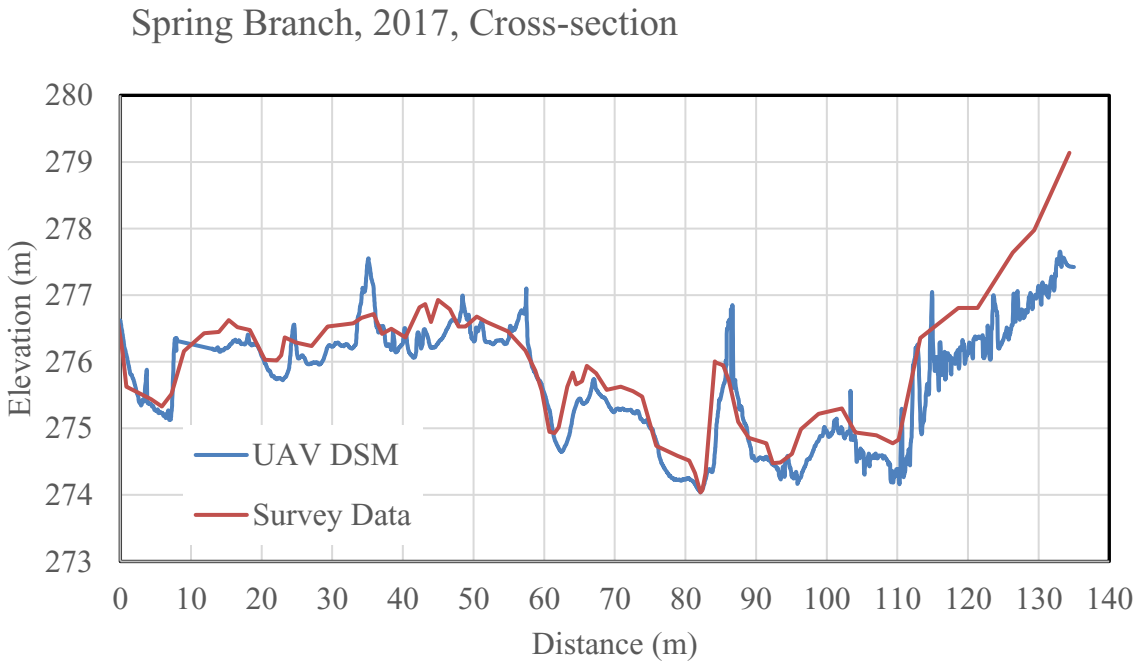
Spring Branch, 2017, Cross-section
Elevation (m)
280
279
278
277
276
275
274
273
UAV DSM
Survey Data
0
10
20
30
40
50
60
70
80
90
100
110
120
130
140
Distance (m)

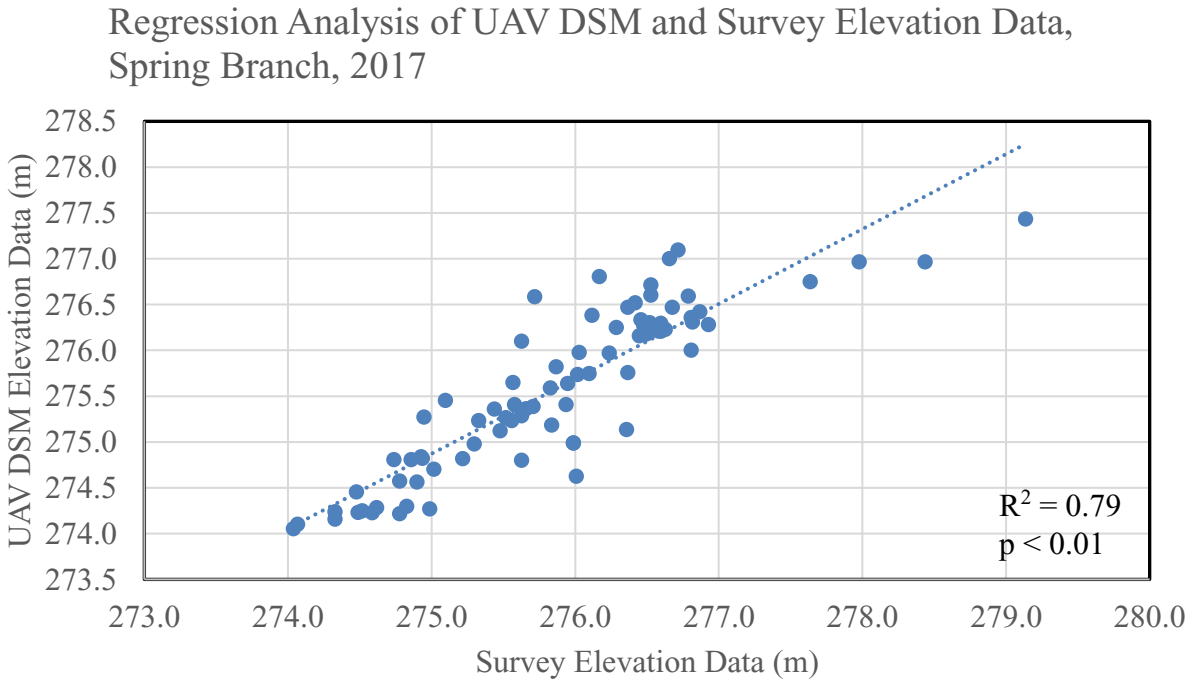
Regression Analysis of UAV DSM and Survey Elevation Data, Spring Branch, 2017
UAV DSM Elevation Data (m)
278.5
278.0
277.5
277.0
276.5
276.0
275.5
275.0
274.5
274.0
273.5
R2 = 0.79
p < 0.01
273.0
274.0
275.0
276.0
277.0
278.0
279.0
280.0
Survey Elevation Data (m)

Lick Branch, 2017, Cross-section

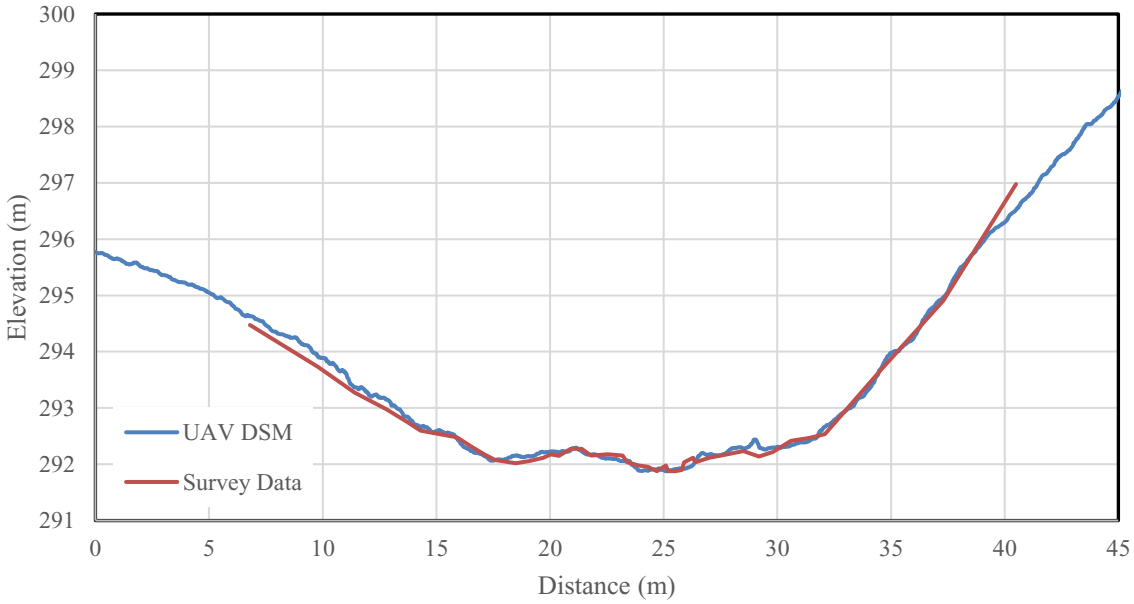

Regression Analysis of UAV DSM and Survey Elevation Data, Lick Branch, 2017